DOT/FAA/AR-01/71

Office of Aviation Research
Washington, D.C. 20591

Damage Resistance Characterization of Sandwich Composites Using Response Surfaces

March 2002

Final Report

This document is available to the U.S. public
through the National Technical Information
Service (NTIS), Springfield, Virginia 22161.

U.S. Department of Transportation
Federal Aviation Administration

20020517 109

1. Report No. DOT/FAA/AR-01/71	2. Government Accession No.	3. Recipient's Catalog No.
4. Title and Subtitle DAMAGE RESISTANCE CHARACTERIZATION OF SANDWICH COMPOSITES USING RESPONSE SURFACES		5. Report Date March 2002
		6. Performing Organization Code
7. Author(s) T.E., Lacy, I.K., Samarah, and J.S. Tomblin,		8. Performing Organization Report No.
9. Performing Organization Name and Address Wichita State University 1845 Fairmount Wichita, KS 67260-0044		10. Work Unit No. (TRAIS)
		11. Contract or Grant No. 00-C-WSU-00-05
12. Sponsoring Agency Name and Address U.S. Department of Transportation Federal Aviation Administration Office of Aviation Research Washington, DC 20591		13. Type of Report and Period Covered Final Report
		14. Sponsoring Agency Code ACE-110
15. Supplementary Notes The FAA William J. Hughes Technical Center Technical Monitor was Peter Shyprykevich.		

16. Abstract

The influence of material configuration and impact parameters on the damage-resistance characteristics of sandwich composites comprised of carbon-epoxy woven fabric facesheets and Nomex honeycomb cores were investigated using empirically based response surfaces. A series of carefully selected tests were used to isolate the coupled influence of number of facesheet plies, core density, core thickness, impact energy, impactor diameter, and impact velocity on the damage formation due to impact normal to the surface. The ranges of selected material parameters were typical of those found in common aircraft applications. The diameter of the planar damage area, which was determined using through transmission ultrasonic (TTU) C-scan measurements and the maximum residual facesheet indentation depth, was used to describe the extent of internal and detectable surface damage, respectively. Estimates of the size of the planar damage region as a function of material system and impact parameters made using quadratic response surface correlated reasonably well with experimentally determined values. For a fixed set of impact parameters, estimates of the planar damage size and residual facesheet indentation suggest that impact damage is highly dependent on skin thickness and core density and thickness. Increasing the thickness of core and decreasing the number of facesheet plies generally resulted in the greatest reduction in the estimated planar damage dimension while increasing the amount of facesheet indentation. An increase in the impactor diameter results in a significant increase in the estimated planar damage size and a decrease in the residual facesheet indentation, particularly for those sandwich panels with thicker facesheets. Thus, blunt object impacts result in appreciable damage that is not detectable using visual inspection. The effects of impact energy and velocity on damage formation were also addressed. As the combinations of material system and impact parameters leading to the maximum estimated internal damage do not correspond to those that result in the greatest facesheet indentation, it may be possible to tailor sandwich composite designs in order to maximize the degree of detectable facesheet damage while minimizing the internal damage associated with expected impacts. These efforts may facilitate sandwich panel design by establishing relationships between material configuration and impact parameters that lead to improved damage tolerance and resistance.

17. Key Words Composites, Sandwich, Honeycomb, Damage tolerance, Damage resistance, Impact, Response surface, Residual strength	18. Distribution Statement This document is available to the public through the National Technical Information Service (NTIS), Springfield, Virginia 22161.	
19. Security Classif. (of this report) Unclassified	20. Security Classif. (of this page) Unclassified	21. No. of Pages 67	22. Price

Form DOT F1700.7 (8-72)   Reproduction of completed page authorized

TABLE OF CONTENTS

LIST OF FIGURES

LIST OF TABLES

EXECUTIVE SUMMARY

The influence of material configuration and impact parameters on the damage-resistance characteristics of sandwich composites comprised of carbon-epoxy woven fabric facesheets and Nomex honeycomb cores were investigated using empirically based response surfaces. A series of carefully selected tests were used to isolate the coupled influence of number of facesheet plies, core density, core thickness, impact energy, impactor diameter, and impact velocity on the damage formation due to impact normal to the surface. The ranges of selected material parameters were typical of those found in common aircraft applications. The diameter of the planar damage area, which was determined by using through transmission ultrasonic (TTU) C-scan measurements and the maximum residual facesheet indentation depth, was used to describe the extent of internal and detectable surface damage, respectively. Estimates of the size of the planar damage region as a function of material system and impact parameters made using quadratic response surface correlated reasonably well with experimentally determined values. For a fixed set of impact parameters, estimates of the planar damage size and residual facesheet indentation suggest that impact damage is highly dependent on skin thickness and core density and thickness. Increasing the thickness of core and decreasing the number of facesheet plies generally resulted in the greatest reduction in the estimated planar damage dimension while increasing the amount of facesheet indentation. An increase in the impactor diameter results in a significant increase in the estimated planar damage size and a decrease in the residual facesheet indentation, particularly for those sandwich panels with thicker facesheets. Thus, blunt object impacts result in appreciable damage that is not detectable using visual inspection. The effects of impact energy and velocity on damage formation were also addressed. As the combinations of material system and impact parameters leading to the maximum estimated internal damage do not correspond to those that result in the greatest facesheet indentation, it may be possible to tailor sandwich composite designs in order to maximize the degree of detectable facesheet damage while minimizing the internal damage associated with expected impacts. These efforts may facilitate sandwich panel design by establishing relationships between material configuration and impact parameters that lead to improved damage tolerance and resistance.

1. INTRODUCTION.

Sandwich construction composites are used in a wide variety of structural applications largely because of their relative advantages over other structural materials in terms of improved stability, weight savings, and ease of manufacture and repair. Sandwich plates and shells are multilayered structures consisting of one or more high-strength, stiff layers (e.g., laminated facings) bonded to one or more flexible layers (core) as shown in figure 1. While the design of structures comprised of sandwich composites is at a fairly mature stage of development [1 to 3], less progress has been made in understanding the effect of adverse in-service impact events on the structural integrity of sandwich structures. Such an understanding is critical where structural durability and damage tolerance are primary considerations. Low-energy impacts may induce localized damage in sandwich composites (fiber breaks, resin cracking, face sheet-core delamination, core crush, puncture, etc.) and can be attributable to a number of fairly common discrete sources (hail, tool drops, runway projectiles, bird strikes, or other unintentional impacts). Any reference to impact damage used herein will suggest the damage associated with relatively low-energy and low-velocity impact events. The effect of intrinsic processing-induced defects (porosity, voids, small disbonds, etc.) and severe damage associated with high-energy impacts resulting from airplane crashes or ballistic events are not considered here.

Characterizing the thermomechanical response of sandwich composites with varying levels of impact damage is a crucial issue in the development of a damage tolerance plan for composite structures. Foreign object impact damage in sandwich composites may result in drastic reductions in composite strength, elastic moduli, durability. An overview of recent investigations into the mechanics of damaged composites may be found in references 4 through 11. The motivation for this study is the development of empirically based models (i.e., response surfaces) that isolate the influence of key material system and lay-up parameters (e.g., number of facesheet plies, facesheet thickness, core thickness, and core density) and impact parameters (e.g., impact energy, spherical impactor diameter, and impact velocity) on the impact damage resistance characteristics of sandwich composites. This effort represents a subset of a somewhat larger combined experimental and modeling investigation into the durability and damage tolerance properties of sandwich composites with varying levels of impact damage [4 and 5]. The focus of this report is on sandwich composites made of plain weave carbon-epoxy facesheets and Nomex honeycomb cores subjected to compression after impact (CAI) loading.
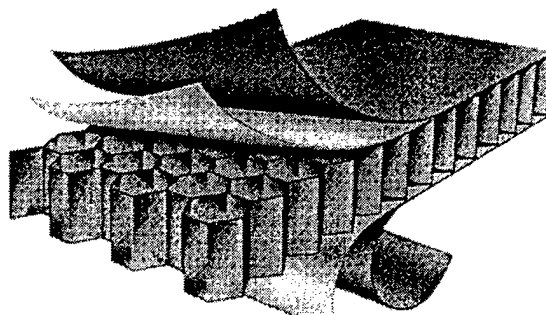
FIGURE 1. TYPICAL SANDWICH COMPOSITE CONSTRUCTION
(From reference 10)

1

2. DAMAGE RESISTANCE CHARACTERIZATION USING EXPERIMENTALLY DETERMINED RESPONSE SURFACES.

In this study, symmetric flat composite sandwich panels comprised of plain weave carbon fabric preimpregnated in epoxy resin (NEWPORT NB321/3K70P) facesheets and Plascore Nomex honeycomb (PN2-3/16-3.0/4.5/6.0) cores (test section dimensions, 8.0 by 8.0 in) with clamped edges were subjected to drop-weight normal impact with a spherical steel impactor. Three different facesheet configurations (X_1 = 2 plies $[90/45]_1$, 4 plies $[90/45]_2$, and 6 plies $[90/45]_3$), core densities (X_2 = 3.0, 4.5, and 6.0 lb/ft^3), and core thicknesses (X_3 = 3/8, 3/4, and 9/8 in) were considered in this examination. The ranges of laminate and core variables are typical of those found in common sandwich panel applications. In addition, three different impact energies (X_4 = 90.0, 120 and 150 in-lb), impactor diameters (X_5 = 1.0, 2.0, and 3.0 in), and impact velocities (X_6 = 65.2, 96.3, and 127 in/sec) were considered in this study. The impact parameters correspond to typical low-velocity impacts associated with relatively blunt objects. Note that each material system and impact variable, X_i (i = 1, 2,.., 6), assumes low, symmetric midrange or center point, and high values; these may be collectively referred to as the natural values of the independent variables used in this study. Table 1 summarizes the range of material system and impact parameters considered in this effort. In addition, the facesheet thickness may be characterized in terms of the number of plies (2, 4, and 6) associated with each facesheet configuration.

TABLE 1. SANDWICH CONFIGURATION AND IMPACT PARAMETERS

		Natural Values		
Material Variables	Number of Facesheet Plies, X_1	2 [90/45]	4 $[90/45]_2$	6 $[90/45]_3$
	Core Density, X_2 (lb/ft^3)	3.0	4.5	6.0
	Core Thickness, X_3 (in)	0.37	0.75	1.12
Impact Variables	Impact Energy, X_4 (in-lb)	90.0	120	150
	Impactor Diameter, X_5 (in)	1.0	2.0	3.0
	Impact Velocity, X_6 (in/sec)	65.2	96.3	127

Consistent with Tomblin, et al. [5], through transmission ultrasonic (TTU) C-scan measurements and maximum residual facesheet indentation, measurements were used to characterize the degree of impact damage induced in the sandwich panels. TTU C-scan measurements provide a two dimensional image of the projected area of the impact damaged region as shown in figure 2. The damaged region may be characterized either in terms of the area of the C-scan image or in terms of the diameter of the damaged region, D, measured normal to the direction of the applied CAI load. Destructive sectioning of impact-damaged sandwich composites comprised of low-density Nomex honeycomb cores (X_2 = 3.0 lb/ft^3) of variable thickness (X_3 = 3/8, 3/4 in) suggests that,

2

for the given facesheet configurations, the planar damage region based upon TTU C-scan measurements closely corresponds to the region over which Nomex honeycomb cell wall buckling/fracture occurs [5]. Furthermore, Tomblin, et al. [5] demonstrated the CAI residual strength of such sandwich composites correlated reasonably well with the projected damage area based upon TTU C-scan measurements for normal impacts involving a range of impactor diameters and impact energies. For example, figure 3 shows the normalized CAI residual strength as a function of projected damage area for symmetric sandwich composites comprised of woven fabric carbon-epoxy facesheets (X_1 = 2 plies [90/45]$_1$, 4 plies [90/45]$_2$, 6 plies [90/45]$_3$) and low-density Nomex honeycomb cores (X_2 = 3.0 lb/ft^3) of variable thickness (X_3 = 3/8, 3/4 in) from reference 5. The panels were impacted with either 1.0-in or 3.0-in-diameter impactors over a range of impact energies. The CAI residual strength of each damaged panel was normalized by the CAI residual strength of an undamaged (virgin) panel of identical configuration. It is clear from the figure that the normalized CAI residual strength is a generally decreasing function of the projected damage area. In addition, the greatest degradation in CAI residual strength is typically associated with those panels impacted with a 3.0-in-diameter impactor for the range of energy levels studied. The latter result is of particular concern because sandwich panels impacted with relatively blunt impactors often display relatively low levels of visible facesheet damage [5]. For a detailed description of the experimental setup and procedure, impact testing, nondestructive and destructive damage evaluation, and CAI testing associated with this effort, please refer to reference 5.
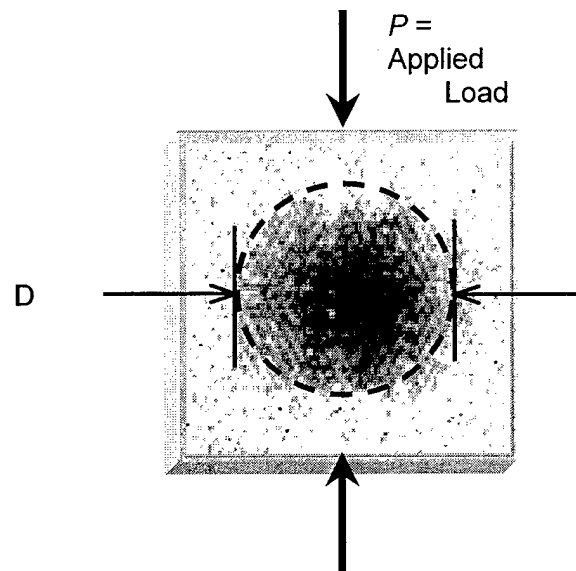
FIGURE 2. TTU C-SCAN IMAGE

One primary goal of this study is to develop empirically based models (i.e., response surfaces) that isolate the influence of key material system/lay-up configuration parameters (e.g., number of facesheet plies or facesheet thickness, X_1; core density, X_2; and core thickness, X_3) and impact parameters (e.g., impact energy, X_4; spherical impactor diameter, X_5; and impact velocity, X_6) on the impact damage induced in sandwich composites. Here, the diameter, D, of the TTU C-scan

area will primarily be used to characterize the level of impact damage (cf., figure 2). Arguably, those combinations of independent variables, X_1-X_6, leading to a reduced value of the diameter, D, of the projected C-scan area for a given impact event may also tend to minimize the degradation in the normalized CAI residual strength for a given panel configuration.
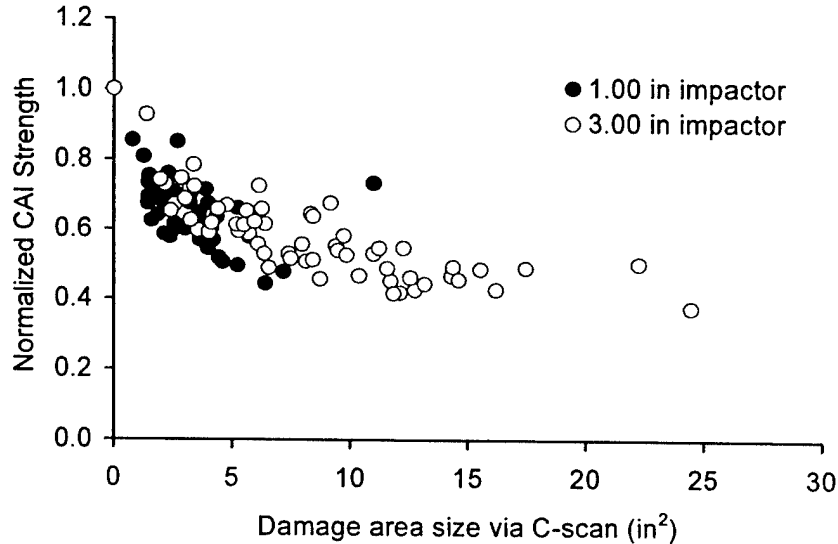
FIGURE 3. NORMALIZED CAI RESIDUAL STRENGTH AS A
FUNCTION OF TTU C-SCAN AREA (From reference 5)

The damage-induced and residual strength degradation in sandwich composites due to foreign object impact is highly configuration- and impact-parameter dependent. Three distinct sets of 15 experiments were conducted in order to isolate the effects of (1) material system/lay-up parameters (X_1-X_3); (2) the number of facesheet plies (X_1), impact energy (X_4), and impactor diameter (X_5); and (3) the number of facesheet plies (X_1), impact energy (X_4), and impact velocity (X_6) on the damage resistance characteristics of sandwich composite panels. In each set of experiments, three of the independent variables were tested at the low, center point, and high-natural levels defined in table 1, and the remaining independent variables were held fixed.

2.1 INFLUENCE OF SKIN AND CORE CONFIGURATION ON THE IMPACT DAMAGE RESISTANCE OF SANDWICH COMPOSITES.

A 3^k fractional factorial design of experiments (DOE) approach [12] has been employed to examine the nonlinear interaction effects between relevant sandwich panel design parameters and their influence on the planar dimension, D, of the damage region associated with a given impact event. In order to isolate the coupled effects of skin and core parameters (i.e., number of facesheet plies, X_1; core density, X_2; core thickness, X_3) on the damage resistance characteristics of sandwich composite panels; the impact energy ($X_4 = 120$ in-lb), impactor diameter ($X_5 = 3.0$ in), and impact velocity ($X_6 = 96.3$ in/sec) were held fixed in this examination. Based on a number of carefully selected experiments, statistically reliable polynomial expressions characterizing the impact damage response of sandwich composites may be determined as a

4

function of relevant test parameters (cf., [12-17]). A quadratic response surface generally will be of the form

$$\hat{D} = b_0 + \sum_{i=1}^{k} b_i \cdot x_i + \sum_{i=1}^{k}\sum_{j=1}^{k} b_{ij} \cdot x_i \cdot x_j \tag{1}$$

where $\hat{D}$ is the predicted response quantity of interest (e.g., damage size), x_i are continuous normalized independent variables, b_0, b_i, and b_{ij} are least squares regression coefficients, and k denotes the number of independent variables considered in the test. The three natural values of the independent variables, X_i, (corresponding to low, midrange/center point, and high values) are mapped into three nondimensionalized or coded levels, x_i, corresponding to (-1, 0, and 1), respectively. In general, the relationship between the natural value and coded level of a given independent variable may be expressed as

$$x_i = \frac{2 \cdot X_i - (X_{iMAX} + X_{iMIN})}{(X_{iMAX} - X_{iMIN})} \tag{2}$$

where X_{iMIN} and X_{iMAX} correspond to the low- and high-natural values of the ith independent variable, respectively. Equation 1 represents a quadratic surface in the k-dimensional space of input parameters and $(x_1, x_2, \ldots x_i, \ldots, x_k) = (0, 0, \ldots, 0, \ldots, 0)$ defines the center point of the test matrix design where independent variables are tested at their midrange values. The constant b_0 represents the average response at the center point of the design, while b_i and b_{ij} contribute to the deviation from this average value at points removed from the center point $(i, j = 1, 2, \ldots, k)$. The test matrices are selected such that the generated response surfaces exhibit a high degree of orthogonality (i.e., only b_0 and b_{ii} are correlated) and rotatability (i.e., the variance of the predicted values at all points equidistant from the center point is constant). One key advantage of this approach is that it allows for estimation of the impact damage response associated with sandwich panel configurations not considered in the original test matrix. In addition, the coupling/interactions between input parameters and their influence on the desired response, $\hat{D}$, may be directly inferred from the magnitudes of the coefficients, b_{ij} $(i \neq j)$.

The test matrix developed for this investigation is based on the Box-Behnken fractional factorial design of experiments technique which uses the minimum number of tests required for generating a second-order, statistically reliable, polynomial expression characterizing the response function of interest (e.g., damage size) [12]. Similar approaches have been used to characterize the fracture toughness, residual strength, and damage tolerance characteristics of composite laminates [18-20]. Table 2 summarizes the natural values and coded levels of the $(k = 3)$ independent variables considered in this particular study. Defining the diameter of the damaged region based upon TTU C-scan measurements as the desired response quantity, $\hat{D}$, equation 1 may be expressed in expanded form, i.e.,

$$\hat{D} = b_0 + b_1 \cdot x_1 + b_2 \cdot x_2 + b_3 \cdot x_3 + b_{11} \cdot x_1^2 + b_{22} \cdot x_2^2 + b_{33} \cdot x_3^2$$
$$\ldots + b_{12} \cdot x_1 \cdot x_2 + b_{13} \cdot x_1 \cdot x_3 + b_{23} \cdot x_2 \cdot x_3 \tag{3}$$

where x_i is the coded level of the ith independent variable $(i = 1, 2, 3)$.

5

TABLE 2. NATURAL VALUES AND CORRESPONDING CODED
LEVELS OF SANDWICH CONFIGURATION VARIABLES

i	Sandwich Variable	Natural Value, X_i	Coded Level, x_i
1	Number of Facesheet Plies	2 [90/45]$_1$	-1
		4 [90/45]$_2$	0
		6 [90/45]$_3$	+1
2	Core Density	3.0 lb/ft^3	-1
		4.5 lb/ft^3	0
		6.0 lb/ft^3	+1
3	Core Thickness	0.37 in	-1
		0.75 in	0
		1.12 in	+1

Consistent with reference 12, the experimental matrix used in this study to solve the regression coefficients (b_0, b_i, and b_{ij}; i, j = 1, 2, 3) required that the high- and low-coded levels of any two independent variables be paired in all possible combinations while fixing the third independent variable at its coded midrange level. These tests are performed in combination with three additional experiments in which the independent variables are fixed at their midrange values ($x_1 = x_2 = x_3 = 0$), resulting in a total of 15 experiments. The latter three center runs are important for assessing the degree of curvature in the response as well as for evaluating model error and goodness of fit. Table 3 shows the test matrix used in this evaluation in terms of the coded levels of the independent variables as well as the measured damage diameter, D, and peak residual facesheet indentation, d, associated with each test. The regression coefficients should be selected such that the error between the predicted estimated values of damage diameter, $\hat{D}$, and the experimentally observed values, D, is minimized over the range of panel configurations tested. The error, e_k, between the predicted and experimentally determined values of the damage diameter for the kth test may be expressed as

$$e_k = D_k - \hat{D}_k \qquad (k = 1, 2, ..., 15) \qquad (4)$$

Using equation 3, the error, e_k, associated with each test may be expressed in terms of the regression coefficients

$$e_k = D_k - \left[b_0 + b_1 \cdot x_1^{(k)} + b_2 \cdot x_2^{(k)} + b_3 \cdot x_3^{(k)} + b_{11} \cdot \left(x_1^{(k)} \right)^2 + b_{22} \cdot \left(x_2^{(k)} \right)^2 \right.$$
$$\left. ... + b_{33} \cdot \left(x_3^{(k)} \right)^2 + b_{12} \cdot x_1^{(k)} \cdot x_2^{(k)} + b_{13} \cdot x_1^{(k)} \cdot x_3^{(k)} + b_{23} \cdot x_2^{(k)} \cdot x_3^{(k)} \right] \qquad (5)$$

for (k = 1, 2, ..., 15). Here $x_i^{(k)}$ represents the specified coded level of the ith independent variable (i = 1, 2, 3) during the kth experimental run (k = 1, 2, ..., 15) from table 3. In the ensuing discussion, it is assumed that the family of errors, e_k (1) are mutually independent in a statistical sense (i.e., the error associated with a given observation will not influence that of any other observation) and (2) are normally distributed about a null mean value and have a common

variance [15]. Furthermore, it is assumed that the predicted response, $\hat{D}$, can be adequately characterized in terms of a quadratic function of independent variables [16].

TABLE 3. CODED SANDWICH CONFIGURATION VARIABLES TEST MATRIX AND MEASURED DAMAGE DIAMETER AND RESIDUAL INDENTATION DEPTH

Test, k	Number of Facesheet Plies, x_1	Core Density, x_2	Core Thickness, x_3	Measured Damage Diameter, D (in)	Measured Residual Indentation Depth, d (in)
1	+1	+1	0	1.96	0.009
2	+1	-1	0	2.08	0.002
3	-1	+1	0	2.29	0.02
4	-1	-1	0	1.99	0.01
5	+1	0	+1	1.73	0.004
6	+1	0	-1	2.83	0.01
7	-1	0	+1	1.63	0.02
8	-1	0	-1	2.37	0.01
9	0	+1	+1	2.06	0.01
10	0	+1	-1	2.76	0.01
11	0	-1	+1	2.08	0.01
12	0	-1	-1	2.00	0.007
13	0	0	0	2.50	0.01
14	0	0	0	2.63	0.01
15	0	0	0	2.47	0.01

The preceding expression (equation 5) may be expressed using compact matrix notation, i.e.,

$$e = D - x \cdot b \qquad (6)$$

Where $\{e\} = (e_1, e_2, ..., e_{15})^T$ is a vector containing the error between the measured and predicted values of the response quantity of interest for all 15 experiments, $\{D\} = (D_1, D_2, ..., D_{15})^T$ is a vector containing the experimentally observed responses (i.e., the measured damage diameters from the last column in table 3), and $\{b\} = (b_0, b_1, b_2, b_3, b_{11}, b_{22}, b_{33}, b_{12}, b_{13}, b_{23})^T$ is a vector containing the desired regression coefficients. The matrix, x, has components

$$[x] = \begin{bmatrix} 1 & x_1^{(1)} & x_2^{(1)} & x_3^{(1)} & \left(x_1^{(1)}\right)^2 & \left(x_2^{(1)}\right)^2 & \left(x_3^{(1)}\right)^2 & x_1^{(1)}\cdot x_2^{(1)} & x_1^{(1)}\cdot x_3^{(1)} & x_2^{(1)}\cdot x_3^{(1)} \\ 1 & x_1^{(2)} & x_2^{(2)} & x_3^{(2)} & \left(x_1^{(2)}\right)^2 & \left(x_2^{(2)}\right)^2 & \left(x_3^{(2)}\right)^2 & x_1^{(2)}\cdot x_2^{(2)} & x_1^{(2)}\cdot x_3^{(2)} & x_2^{(2)}\cdot x_3^{(2)} \\ \vdots & \vdots & \vdots & \vdots & \vdots & \vdots & \vdots & \vdots & \vdots & \vdots \\ 1 & x_1^{(15)} & x_2^{(15)} & x_3^{(15)} & \left(x_1^{(15)}\right)^2 & \left(x_2^{(15)}\right)^2 & \left(x_3^{(15)}\right)^2 & x_1^{(15)}\cdot x_2^{(15)} & x_1^{(15)}\cdot x_3^{(15)} & x_2^{(15)}\cdot x_3^{(15)} \end{bmatrix} \quad (7)$$

where $x_i^{(k)}$ denotes the value of the ith independent variable ($i = 1, 2, 3$) specified in the kth experimental test. Using the prescribed values of the coded independent variables for the test matrix specified in table 3, the matrix, x, may be expressed as

$$[x] = \begin{bmatrix} 1 & 1 & 1 & 0 & 1 & 1 & 0 & 1 & 0 & 0 \\ 1 & 1 & -1 & 0 & 1 & 1 & 0 & -1 & 0 & 0 \\ 1 & -1 & 1 & 0 & 1 & 1 & 0 & -1 & 0 & 0 \\ 1 & -1 & -1 & 0 & 1 & 1 & 0 & 1 & 0 & 0 \\ 1 & 1 & 0 & 1 & 1 & 0 & 1 & 0 & 1 & 0 \\ 1 & 1 & 0 & -1 & 1 & 0 & 1 & 0 & -1 & 0 \\ 1 & -1 & 0 & 1 & 1 & 0 & 1 & 0 & -1 & 0 \\ 1 & -1 & 0 & -1 & 1 & 0 & 1 & 0 & 1 & 0 \\ 1 & 0 & 1 & 1 & 0 & 1 & 1 & 0 & 0 & 1 \\ 1 & 0 & 1 & -1 & 0 & 1 & 1 & 0 & 0 & -1 \\ 1 & 0 & -1 & 1 & 0 & 1 & 1 & 0 & 0 & -1 \\ 1 & 0 & -1 & -1 & 0 & 1 & 1 & 0 & 0 & 1 \\ 1 & 0 & 0 & 0 & 0 & 0 & 0 & 0 & 0 & 0 \\ 1 & 0 & 0 & 0 & 0 & 0 & 0 & 0 & 0 & 0 \\ 1 & 0 & 0 & 0 & 0 & 0 & 0 & 0 & 0 & 0 \end{bmatrix} \quad (8)$$

The vector equation (6) may be expressed graphically in the 15-dimensional space of the experimental observations as shown in figure 4. In order to minimize the magnitude of the vector of errors, the error vector associated with all of the experimental observations, e, should be orthogonal to the vector of predicted responses, $x \cdot b$, i.e.,

$$(x \cdot b) \cdot e = 0 \quad (9)$$

or equivalently from equation 6

$$(x \cdot b) \cdot (D - x \cdot b) = 0 \quad (10)$$

8
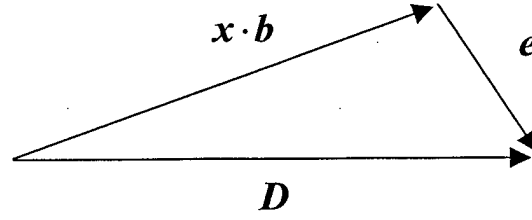
FIGURE 4. VECTOR REPRESENTATION OF THE MODEL ERROR

The latter expression may be directly solved for the vector containing the desired regression coefficients, i.e.,

$$b = (x^T \cdot x)^{-1} \cdot (x^T \cdot D)$$ (11)

The vector, b, is commonly referred to as the Least Squares Estimate of the model parameters vector. This estimate is unbiased and has the minimum variance among all other types of unbiased estimators [15]. Using equations 9 and 11 in combination with the vector, D, of observed responses from table 3, the components of the model parameters vector may be readily determined, i.e.,

$$\{b\} = \begin{Bmatrix} b_0 \\ b_1 \\ b_2 \\ b_3 \\ b_{11} \\ b_{22} \\ b_{33} \\ b_{12} \\ b_{13} \\ b_{23} \end{Bmatrix} = \begin{Bmatrix} 2.538 \\ 0.04188 \\ 0.1138 \\ -0.3069 \\ -0.2674 \\ -0.1857 \\ -0.1264 \\ -0.1048 \\ -0.09000 \\ -0.1958 \end{Bmatrix} \text{ (in)}$$ (12)

Hence, the quadratic response surface characterizing the diameter of the damage area based upon TTU C-scan measurements in terms of coded levels of the composite sandwich panel facesheet thickness (x_1), core density (x_2), and core thickness (x_3) may be expressed as

$$\hat{D} = 2.538 + 0.04188 \cdot x_1 + 0.1138 \cdot x_2 - 0.3069 \cdot x_3$$
$$... - 0.2674 \cdot x_1^2 - 0.1857 \cdot x_2^2 - 0.1264 \cdot x_3^2 \quad \text{(in)}$$ (13)
$$... - 0.1048 \cdot x_1 \cdot x_2 - 0.09000 \cdot x_1 \cdot x_3 - 0.1958 \cdot x_2 \cdot x_3$$

9

The constant term ($b_0 = 2.53$ in) represents the mean diameter of the TTU C-scan image for those panels corresponding to the center point of the design. Note that, based upon the magnitudes of the coefficients of the linear terms in equation 13, the coded core thickness, x_3, contributes the most to the linear variation in the predicted response at points removed from the center point (x_1, x_2, x_3) = (0, 0, 0) of the designed test matrix (e.g., increasing the core thickness from its midrange value will result in a linear decrease in the predicted damage diameter from b_0; conversely, decreasing the core thickness from its midrange value will result in a linear increase in the predicted response). Similarly, an increase in the number of facesheet plies, x_1, or in the core density, x_2, will contribute to a linear increase in the diameter of the projected damaged region. Based upon the coefficients of the quadratic terms, variations in the independent variables away from their midrange values will result in a quadratic decrease in the predicted damage diameter. Due to the normalization procedure used in defining the coded variables (equation 2), the influence of the quadratic terms on the predicted response will be maximized as the coded variables approach their extreme values ($x_i = \pm 1$). The coefficients of the interaction terms ($x_i \cdot x_j$; $i \neq j$) provide an indication of the complex coupling between sandwich panel parameters and their influence on its damage resistance characteristics. In this case, simultaneously increasing or decreasing any two independent variables will result in a bilinear decrease in the predicted response away from its mean center point value. Similarly, increasing one independent variable while simultaneous reducing another will result in a bilinear increase in the predicted damage size. It is clear from the functional form of the response surface, (equation 13) that, for the given range of material and impact parameters, the impact damage induced is sandwich configuration dependent. Using the response surface methodology outlined here, it may be possible to identify nonlinear interaction effects involving multiple independent variables that could not have been ascertained easily by traditional single-variable test strategies and analysis. Such approaches may facilitate sandwich panel design by establishing relationships between material and/or configuration parameters that lead to improved damage tolerance/ resistance.

Following the same procedure that was used to develop the response surface (equation 13) and using the observed residual facesheet indentation data in table 3, a quadratic response surface characterizing the peak residual facesheet indentation, $\hat{d}$, in terms of coded levels of the composite sandwich panel facesheet thickness (x_1), core density (x_2), and core thickness (x_3) was developed of the form

$$\hat{d} = [15.00 - 5.750 \cdot x_1 + 2.250 \cdot x_2 + 0.2500 \cdot x_3$$
$$... - 0.3750 \cdot x_1^2 - 2.875 \cdot x_2^2 - 0.8750 \cdot x_3^2 \qquad \text{(in)} \qquad (14)$$
$$... - 0.2500 \cdot x_1 \cdot x_2 - 3.250 \cdot x_1 \cdot x_3 - 1.750 \cdot x_2 \cdot x_3] \cdot 10^{-3}$$

The constant term ($b_0 = 0.015$ in) represents the mean value of the peak residual facesheet indentation for the three center runs. As might be expected, the coded facesheet thickness, x_1, contributes the most to the linear variation in the predicted response at points removed from the center point of the test matrix (e.g., increasing x_1 from its midrange value will result in a linear decrease in the predicted damage diameter from b_0; conversely, decreasing x_1 from its midrange value will result in a linear increase in $\hat{d}$). Similar arguments can be made when interpreting the influence of the remaining terms in equation 14 on the predicted response. Note that the Box-Behnken test matrix defined in table 3 represents a spherical experimental design, i.e., the

10

first 12 tests are conducted at points (x_1, x_2, x_3) that are equidistant from the center point of the design. If one considers a cube in the space of the coded variables defined by the planes $(x_1 = \pm 1, x_2 = \pm 1, x_3 = \pm 1)$, the noncenter point tests are conducted at edge points (i.e., points located at the centers of the edges of the cube) as shown schematically in figure 5. Hence, the edge points all lie a coded radial distance $r = \sqrt{x_1^2 + x_2^2 + x_3^2} = \sqrt{2} = 1.414$ from the center point of the design. When using response surfaces, such as equation 12, to estimate the impact damage response associated with panel configurations not considered in the original test matrix, special care must be used to ensure that the interpolation occurs within the spherical domain defined by the coded radius, $r = \sqrt{2}$. Extrapolation to panel configurations that lie outside this spherical region may lead to serious errors in the predicted response. If response surface estimates are desired over a cuboidal domain, then various other experimental designs may be employed (e.g., Central Composites Design, see reference 15).

While the interpretation of the regression coefficients is most easily performed if a response surface is characterized in terms of the coded levels of the independent variables, equation 2 may be used to rewrite the response surfaces (equations 13 and 14) in terms of the natural values of the independent variables, i.e.,

$$\hat{D} = -2.682 + 0.8029 \cdot X_1 + 1.219 \cdot X_2 + 2.576 \cdot X_3$$
$$... - 0.06685 \cdot X_1^2 - 0.08252 \cdot X_2^2 - 0.8990 \cdot X_3^2 \qquad \text{(in)} \qquad (15)$$
$$... - 0.03492 \cdot X_1 \cdot X_2 - 0.1200 \cdot X_1 \cdot X_3 - 0.3480 \cdot X_2 \cdot X_3$$

and

$$\hat{d} = \big[-36.63 + 1.500 \cdot X_1 + 15.67 \cdot X_2 + 41.33 \cdot X_3$$
$$... - 0.09375 \cdot X_1^2 - 1.278 \cdot X_2^2 - 6.222 \cdot X_3^2 \qquad \text{(in)} \qquad (16)$$
$$... - 0.08333 \cdot X_1 \cdot X_2 - 4.333 \cdot X_1 \cdot X_3 - 3.111 \cdot X_2 \cdot X_3 \big] \cdot 10^{-3}$$

The latter representations allow the response surfaces to be plotted in the space of the natural variables. Ostensibly, the response surface (equation 14 or 16) may be used to identify those panel configurations that lead to appreciable levels of visibly detectable damage. Tomblin, et al. [5], however, demonstrated that there may be no correlation between the peak residual facesheet indentation depth and residual strength degradation in impact-damaged sandwich panels. Identification of those sandwich panel configurations that tend to minimize the planar damage area associated with a given impact event, however, has the potential to result in a more damage-tolerant sandwich panel design. Hence, characterization of the size of the planar damage region associated with impact, D, was the central focus of this effort.

2.1.1 Discussion of Sandwich Configuration Regression Model Results.

The response surfaces (equations 13 through 16) were used to assess which combinations of sandwich configuration parameters lead to the minimum (or maximum) level of impact damage for the specified impact. Table 4 summarizes the measured and predicted planar TTU C-scan

11

diameter (damage diameter) and the maximum residual facesheet indentation (damage depth) for the sandwich composite panels considered. "Predicted" as used in this discussion, describes the response surface estimate to the measured data. The difference between the experimentally measured damage diameters and the predicted values, using equation 13, varied between 1.3% and 15.5% for the 15 panels tested, with a mean difference of 5.8%. This suggests that the response surface in equation 13 provides a reasonable characterization of the influence of the number of facesheet plies, core density, and core thickness have on the size of the internal damage generated due to impact. The regression results may also be viewed schematically in the space of coded independent variables as shown in figure 5. For the relatively blunt object impacts (3.0-in-diameter impactor) considered in this study, the experimentally measured peak residual facesheet indentations were on the order of the ply thickness (i.e., 0.002-0.022 in). While the magnitudes of the differences between the measured and predicted indentation depths were reasonably small in comparison to the typical ply thickness, the percentage difference between the two values was fairly significant, particularly for those shallow indentations approaching the limits of mechanical measurement (see reference 5). For this reason, response surface estimates of the peak indentation depth are likely inaccurate for the class of blunt object impacts considered here, particularly for the extremely shallow indentation profile cases. Note that, if there is significant scatter in the experimental results associated with the center point runs, then this will be reflected in the specification of the constant term b_0 in the response surface in equation 3. Ideally, the experimental center point observations should be tightly banded about their mean value, b_0, in order to avoid introducing a large degree of uncertainty into the regression model. This is a particular concern when assessing the residual facesheet indentation, where the experimental observations may not be particularly repeatable.

TABLE 4. COMPARISONS BETWEEN PREDICTED AND MEASURED DAMAGE SIZES
(From tests 1 to 15)

Test, k	x_1	x_2	x_3	Measured Damage Diameter, D (in)	Predicted Damage Diameter, $\hat{D}$ (in)	$\left\lvert\dfrac{D-\hat{D}}{D}\right\rvert$ (%)	Measured Damage Depth, d (in)	Predicted Damage Depth, $\hat{d}$ (in)	$\left\lvert\dfrac{d-\hat{d}}{d}\right\rvert$ (%)
1	+1	+1	0	1.96	2.13	8.7	0.009	0.008	11.1
2	+1	-1	0	2.08	2.11	1.5	0.002	0.004	100
3	-1	+1	0	2.29	2.26	1.4	0.022	0.020	9.1
4	-1	-1	0	1.99	1.82	8.6	0.014	0.015	7.1
5	+1	0	+1	1.73	1.78	3.0	0.004	0.005	25.0
6	+1	0	-1	2.83	2.58	8.9	0.013	0.011	15.4
7	-1	0	+1	1.63	1.88	15.5	0.021	0.023	9.5
8	-1	0	-1	2.37	2.31	2.2	0.017	0.016	5.9
9	0	+1	+1	2.06	1.83	10.8	0.012	0.012	0.0
10	0	+1	-1	2.76	2.84	3.0	0.012	0.015	25.0
11	0	-1	+1	2.08	2.0	4.0	0.014	0.011	21.4
12	0	-1	-1	2.0	2.22	11.1	0.007	0.007	0.0
13	0	0	0	2.50	2.53	1.3	0.013	0.015	15.4
14	0	0	0	2.63	2.53	3.7	0.017	0.015	11.8
15	0	0	0	2.47	2.53	2.7	0.015	0.015	0.0
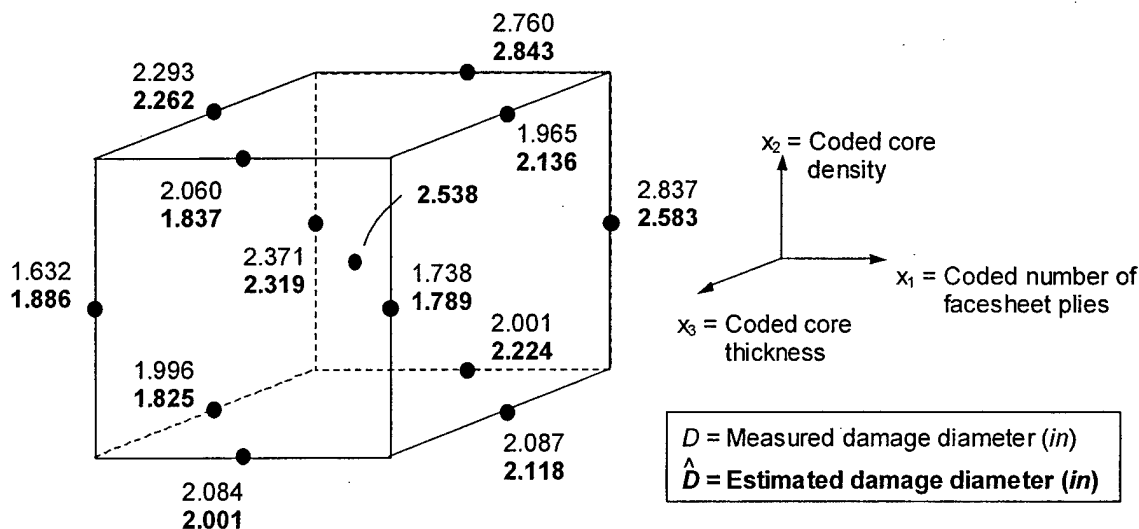
FIGURE 5. RESPONSE SURFACE ESTIMATES OF THE INTERNAL DAMAGE
DIAMETER AS A FUNCTION OF SANDWICH CONFIGURATION PARAMETERS

Nonetheless, consideration of the response surface in equation 14 may help identify key combinations of material system configuration parameters that lead to improved damage resistance properties. As part of continuing efforts associated with this study, standard analysis of variance, error estimation, and goodness of fit, checks will be performed in order to fully validate the approach outlined here.

Figures 6 through 11 summarize the influence of the number of facesheet plies (X_1, x_1), core density (X_2, x_2), and core thickness (X_3, x_3) on the size of the planar damage region. In each of the response surface plots contained in this report, the bounds of the sphere of coded radius, $r = \sqrt{2}$, is denoted by an inscribed dashed circle. Strictly speaking, discussion of regression data falling outside the bounds of this sphere would correspond to an extrapolation of the response surface results. In addition, it is important to recognize that the influence of the number of facesheet plies (i.e., thickness) should only be evaluated at $X_1 = 2$, 4, and 6 plies (or $x_1 = -1$, 0, 1) since interpolation between the 2-, 4-, and 6-ply configurations considered here would lead to aphysical results. Figures 6(a), 6(b), and 6(c) show the estimated damage diameter (equation 15) as a function of facesheet thickness and core density for core thickness values of $X_3 = 3/8$, 3/4, and 9/8 in (or $x_3 = -1$, 0, 1), respectively. It is clear from figure 6(a) that, for sandwich panels with the minimum core thickness ($X_3 = 3/8$ in; $x_3 = -1$), the damage diameter generally increases with increasing core density, X_2, and number of facesheet plies, X_1. The minimum damage occurs in the vicinity of $X_1 = 2$ plies and $X_2 = 3.0$ lb/ft^3 (or $x_1 = x_2 = -1$) where the penetration resistance is somewhat reduced and damage development is likely to be more localized. Note that, as the core thickness is increased to its midrange value ($X_3 = 3/4$ in; $x_3 = 0$), both the magnitude of the peak damage diameter and its location in the space of independent variables changes (figure 6(b)). Here, the peak predicted damage diameter is in the vicinity of the center point of the design; the damage is a relative minimum for $X_1 = 2$, 6 plies ($x_1 = \pm 1$) and $X_2 = 3.0$, 6.0 lb/ft^3 ($x_2 = \pm 1$), corresponding to the extreme ranges of the tested values. This latter result is in agreement with the experimental observations. Figure 7 shows the TTU C-scan images and

13

recorded damage diameters for the test specimens corresponding to the midrange core thickness configurations ($x_3 = 0$; $X_3 = 3/4$ in). Consistent with the regressions of figure 6(b), the recorded damage diameter was a maximum at the center point of the design (x_1, x_2, x_3) = (0, 0, 0) or (X_1, X_2, X_3) = (4 plies, 4.5 lb/ft^3, 3/4 in), and a relative minimum at extreme values of facesheet thickness and core density. Figure 6(c) shows that as the core thickness is increased to its maximum value ($X_3 = 9/8$ in; $x_3 = 1$), the peak damage diameter is reduced by roughly 17% from the case where $X_3 = 3/4$ in ($x_3 = 0$) (figure 6(b)). Note that, as the core thickness is increased from $X_3 = 3/8$ in to $X_3 = 9/8$ in ($x_3 = -1$, 1), the magnitude of the peak damage is significantly reduced and the location of the maximum transitions from approximately (X_1, X_2) = (4 plies, 6.0 lb/ft^3) to near the center point of the design parameters considered. There is likely a competition between enhanced penetration resistance and improved bending stiffness associated with changes in independent variables that govern the damage development. Such influences, while difficult to ascertain using traditional single-variable test strategies and analysis, are readily identified using carefully developed response surfaces.

Figures 8(a), 8(b), and 8(c) show the estimated damage diameter (equation 15) as a function of facesheet thickness and core thickness for core density values of $X_2 = 3.0$, 4.5, and 6.0 lb/ft^3 or $x_2 = -1$, 0, 1, respectively. Similar to the preceding case, increasing the thickness of the core tends to markedly reduce the magnitude of the estimated damage. It is likely that the enhanced bending stiffness provided by increasing the core thickness reduces the global deformation during impact that can lead to larger-scale core crushing. The lower the penetration resistance of the sandwich composite, the more likely the damage is to be confined to a localized region in the vicinity of the contact area associated with the impactor. This may explain the fairly low predicted damage diameter in the vicinity of X_1, X_2, X_3 = 2 plies, 3.0 lb/ft^3, 9/8 in or x_1, x_2, x_3 = -1, -1, 1) corresponding to the minimum facesheet thickness and core density, and maximum core thickness (figure 8(a)). Note that increasing the number of facesheet plies from $X_1 = 2$ plies to $X_1 = 4$ plies will increase the penetration resistance of the sandwich composite. If such an increase is not accompanied by an appropriate increase in the bending stiffness, then the deformation due to impact may become distributed over a wider area resulting in an increase in the internal damage. This may explain why increasing the number of facesheet plies from low to midrange levels tends to increase the estimated damage, particularly when the core thickness is a minimum. Note that increasing the number of plies from $X_1 = 4$ plies to $X_1 = 6$ plies tends to decrease the predicted damage size; this may be a result of the enhanced bending stiffness provided by the facesheets. Figure 9 shows the TTU C-scan images and recorded damage diameters for the test specimens corresponding to the midrange core density configurations ($x_2 = 0$; $X_2 = 4.5$ lb/ft^3). Consistent with the regression of figure 8(b), the recorded damage diameters decreased sharply with increasing core thickness and increased as the number of facesheet plies was increased from low to center point values. A comparison of figures 8(a) through 8(c) suggests that increasing the core density will tend to increase the damage induced, especially for the case where the facesheet thickness is a minimum. Similar to the preceding case, both the magnitude of the peak damage size and its location in the space of independent variables changes with increasing core density.

(a)

(b)

Increasing core thickness, X_3

(c)
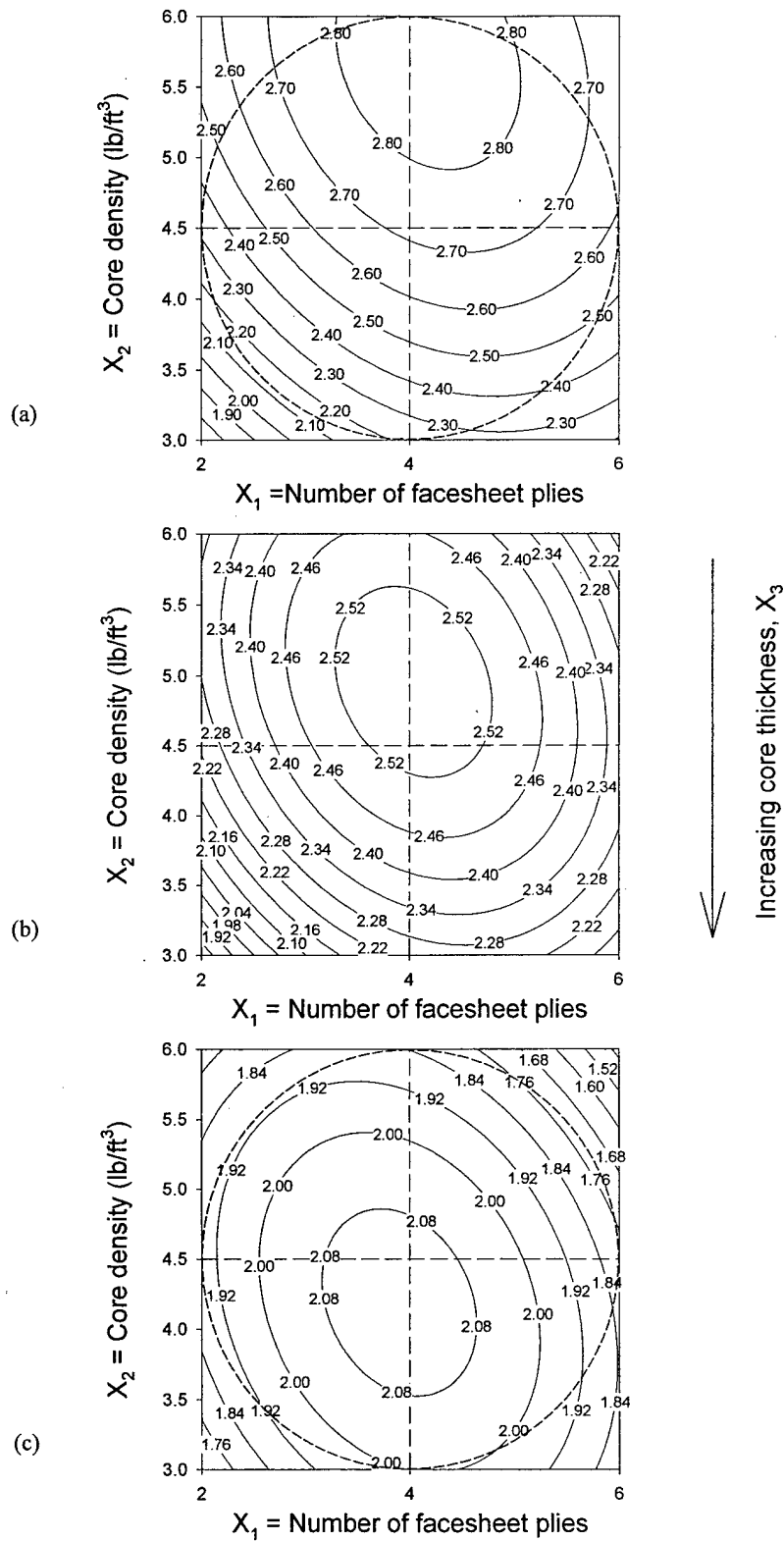
FIGURE 6. PREDICTED DAMAGE DIAMETER (in): (a) $X_3 + 0.37$ in;
(b) $X_3 = 0.75$ in; and (c) $X_3 = 1.12$ in

15

TEST # 3 $D = 2.293\ in$
$\begin{Bmatrix} x_1 \\ x_2 \\ x_3 \end{Bmatrix} = \begin{Bmatrix} -1 \\ +1 \\ 0 \end{Bmatrix}$

Increasing facesheet thickness, x_1

TEST # 1 $D = 1.965\ in$
$\begin{Bmatrix} x_1 \\ x_2 \\ x_3 \end{Bmatrix} = \begin{Bmatrix} +1 \\ +1 \\ 0 \end{Bmatrix}$

Increasing facesheet thickness and core density

Increasing core density, x_2

TEST # 13 $D = 2.506\ in$
$\begin{Bmatrix} x_1 \\ x_2 \\ x_3 \end{Bmatrix} = \begin{Bmatrix} 0 \\ 0 \\ 0 \end{Bmatrix}$

TEST # 15 $D = 2.472\ in$
$\begin{Bmatrix} x_1 \\ x_2 \\ x_3 \end{Bmatrix} = \begin{Bmatrix} 0 \\ 0 \\ 0 \end{Bmatrix}$

TEST # 14 $D = 2.637\ in$
$\begin{Bmatrix} x_1 \\ x_2 \\ x_3 \end{Bmatrix} = \begin{Bmatrix} 0 \\ 0 \\ 0 \end{Bmatrix}$

$b_0 = 2.538\ in$

Increasing core density, x_2

Increasing facesheet thickness and core density.

TEST # 4 $D = 1.996\ in$
$\begin{Bmatrix} x_1 \\ x_2 \\ x_3 \end{Bmatrix} = \begin{Bmatrix} -1 \\ -1 \\ 0 \end{Bmatrix}$

Increasing facesheet thickness, x_1

TEST # 2 $D = 2.087\ in$
$\begin{Bmatrix} x_1 \\ x_2 \\ x_3 \end{Bmatrix} = \begin{Bmatrix} +1 \\ -1 \\ 0 \end{Bmatrix}$

FIGURE 7. MEASURED DAMAGE DIAMETER FOR CORE THICKNESS,
$X_3 = 3/4$ in ($x_3 = 0$)

FIGURE 8. PREDICTED DAMAGE DIAMETER (in): (a) $X_2 = 3.0 \text{ lb/ft}^3$;
(b) $X_2 = 4.5 \text{ lb/ft}^3$; and (c) $X_2 = 6.0 \text{ lb/ft}^3$

TEST # 7 $D = 1.632\,in$

$$\begin{Bmatrix} x_1 \\ x_2 \\ x_3 \end{Bmatrix} = \begin{Bmatrix} -1 \\ 0 \\ +1 \end{Bmatrix}$$

Increasing facesheet thickness, x_1

TEST # 5 $D = 1.738\,in$

$$\begin{Bmatrix} x_1 \\ x_2 \\ x_3 \end{Bmatrix} = \begin{Bmatrix} +1 \\ 0 \\ +1 \end{Bmatrix}$$

Increasing facesheet thickness and core thickness.

Increasing core thickness, x_3

TEST # 13 $D = 2.506\,in$

$$\begin{Bmatrix} x_1 \\ x_2 \\ x_3 \end{Bmatrix} = \begin{Bmatrix} 0 \\ 0 \\ 0 \end{Bmatrix}$$

TEST # 15 $D = 2.472\,in$

$$\begin{Bmatrix} x_1 \\ x_2 \\ x_3 \end{Bmatrix} = \begin{Bmatrix} 0 \\ 0 \\ 0 \end{Bmatrix}$$

TEST # 14 $D = 2.637\,in$

$$\begin{Bmatrix} x_1 \\ x_2 \\ x_3 \end{Bmatrix} = \begin{Bmatrix} 0 \\ 0 \\ 0 \end{Bmatrix}$$

$b_0 = 2.538\,in$

Increasing core thickness, x_3

Increasing facesheet thickness and core thickness.

TEST # 8 $D = 2.371\,in$

$$\begin{Bmatrix} x_1 \\ x_2 \\ x_3 \end{Bmatrix} = \begin{Bmatrix} -1 \\ 0 \\ -1 \end{Bmatrix}$$

Increasing facesheet thickness, x_1

TEST # 6 $D = 2.837\,in$

$$\begin{Bmatrix} x_1 \\ x_2 \\ x_3 \end{Bmatrix} = \begin{Bmatrix} +1 \\ 0 \\ -1 \end{Bmatrix}$$

FIGURE 9. MEASURED DAMAGE DIAMETER FOR CORE DENSITY,
$X_2 = 4.5\ lb/ft^3$ ($x_2 = 0$)

Figures 10(a), 10(b), and 10(c) show the estimated damage diameter (equation 15) as a function of core density and core thickness for 2-, 4-, and 6-ply facesheet configurations (or $x_1 = -1, 0, 1$), respectively. A comparison of the three figures reveals that the predicted damage size is sensitive to the number of facesheet plies. Similar to the preceding results, the estimated damage tends to decrease rapidly with increasing core thickness and increase somewhat with increasing core density. Figure 11 shows that the TTU C-scan images and recorded damage diameters for the test specimens corresponding to the midrange facesheet configurations ($x_1 = 0$; $X_1 = 4$ plies) are consistent with the regressions of figure 10(b).

18

FIGURE 10. PREDICTED DAMAGE DIAMETER (in): (a) X_1 = 2 plies $[90/45]_1$;
(b) X_1 = 4 plies $[90/45]_2$; and (c) X_1 = 6 plies $[90/45]_3$

$$\begin{Bmatrix} x_1 \\ x_2 \\ x_3 \end{Bmatrix} = \begin{Bmatrix} 0 \\ -1 \\ +1 \end{Bmatrix}$$

Increasing core density, x_2

$$\begin{Bmatrix} x_1 \\ x_2 \\ x_3 \end{Bmatrix} = \begin{Bmatrix} 0 \\ +1 \\ +1 \end{Bmatrix}$$

TEST # 11 $D = 2.084\ in$

TEST # 9 $D = 2.060\ in$

Increasing core thickness and core density.

Increasing core thickness, x_3

$$\begin{Bmatrix} x_1 \\ x_2 \\ x_3 \end{Bmatrix} = \begin{Bmatrix} 0 \\ 0 \\ 0 \end{Bmatrix}$$

TEST # 13 $D = 2.506\ in$

$$\begin{Bmatrix} x_1 \\ x_2 \\ x_3 \end{Bmatrix} = \begin{Bmatrix} 0 \\ 0 \\ 0 \end{Bmatrix}$$

TEST # 15 $D = 2.472\ in$

Increasing core thickness, x_3

$$\begin{Bmatrix} x_1 \\ x_2 \\ x_3 \end{Bmatrix} = \begin{Bmatrix} 0 \\ 0 \\ 0 \end{Bmatrix}$$

$b_0 = 2.538\ in$

TEST # $D = 2.637\ in$

Increasing core thickness and core density.

$$\begin{Bmatrix} x_1 \\ x_2 \\ x_3 \end{Bmatrix} = \begin{Bmatrix} 0 \\ -1 \\ -1 \end{Bmatrix}$$

Increasing core density, x_2

$$\begin{Bmatrix} x_1 \\ x_2 \\ x_3 \end{Bmatrix} = \begin{Bmatrix} 0 \\ +1 \\ -1 \end{Bmatrix}$$

TEST # 12 $D = 2.001\ in$

TEST # 10 $D = 2.760\ in$

FIGURE 11. MEASURED DAMAGE DIAMETER FOR FACESHEET CONFIGURATION, $X_1 = 4$ plies $[90/45]_2$ $(x_1 = 0)$

Figures 12 through 14 summarize the influence of the independent variables on the maximum residual facesheet indentation. Figures 12(a), 12(b), and 12(c) show the estimated indentation depth (equation 16) as a function of facesheet thickness and core density for core thickness values of X_3 = 3/8, 3/4, and 9/8 in (or x_3 = -1, 0, 1). As might be expected, figure 12 suggests that the predicted indentation depth decreases sharply as the number of facesheet plies increases. For the minimum thickness core (figure 12(a)), increasing the core density resulted in a sharp increase in the estimated indentation depth for a given facesheet configuration. The estimates became somewhat less sensitive to the core density as the core thickness was increased (see figures 12(b) and 12(c)). In contrast to the estimates of the diameter of the planar damage region, increasing the core thickness tends to increase the predicted indentation damage for the minimum (2-ply) facesheet configuration. This makes sense given the reduced penetration resistance associated with the decreasing facesheet thickness.

Figures 13(a), 13(b), and 13(c) show the predicted indentation depth (equation 16) as a function of the number of facesheet plies and core thickness for core density values of X_2 = 3.0, 4.5, and 6.0 lb/ft^3 (or x_2 = -1, 0, 1). Similar to the preceding case, increasing the number of facesheet plies markedly reduces the magnitude of the estimated indentation damage. For the minimum core density (figure 13(a)), the estimated damage depth tends to increase with increasing core thickness. For midrange and high levels of core density (figures 13(b) and 13(c), respectively), the predicted indentation depth is largely dominated by the number of facesheet plies.

Figures 14(a), 14(b), and 14(c) show the estimated indentation depth (equation 16) as a function of core density and core thickness for the 2-, 4-, and 6-ply facesheet configurations. A comparison of the three figures reveals that the predicted damage size is highly sensitive to the number of facesheet plies. While the estimates tend to increase with increasing core density for all three facesheet configurations, the point X_1 = 2 plies (x_1 = 0) appears to be near an inflection in the response surface. For the minimum number of facesheet plies, the peak damage corresponds roughly to (X_2, X_3) = (4.5 lb/ft^3, 9/8 in) or (x_2, x_3) = (0, 1). For the 6-ply facesheet configuration, the peak damage corresponds roughly to (X_2, X_3) = (6.0 lb/ft^3, 3/8 in) or (x_2, x_3) = (1, -1). The coupled influence of the three material parameters would be difficult to discern using a traditional single variable testing strategy. Note that the trends illustrated in figures 12 through 14 are consistent with the residual indentation depth measurements summarized in table 4. A critical comparison of figures 6, 8, and 10 to figures 12, 13, and 14 suggests that those combinations of sandwich configuration parameters that lead to the maximum amount of internal damage (and possibly the greatest relative reduction in residual strength [5]) do not correspond to the configurations that produce the greatest facesheet indentation (i.e., damage conditions that are amenable to visual inspection). This is a serious issue in the development of a damage tolerance plan for sandwich composites.

FIGURE 12. PREDICTED RESIDUAL INDENTATION DEPTH (in): (a) $X_3 = 0.37$ in; (b) $X_3 = 0.75$ in; and (c) $X_3 = 1.12$ in

22

FIGURE 13. PREDICTED RESIDUAL INDENTATION DEPTH (in): (a) $X_2 = 3.0$ lb/ft^3; (b) $X_2 = 4.5$ lb/ft^3; and (c) $X_2 = 6.0$ lb/ft^3
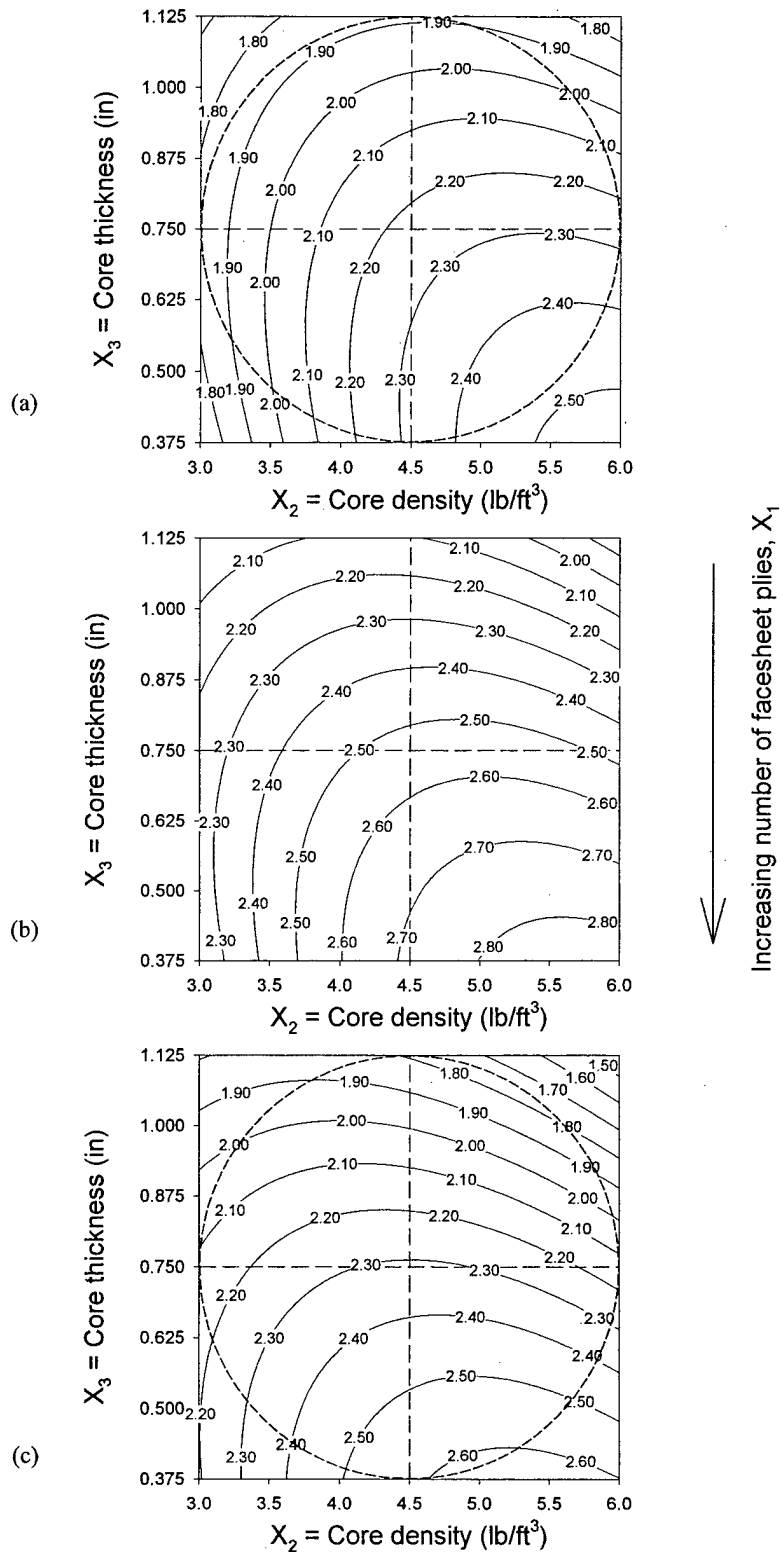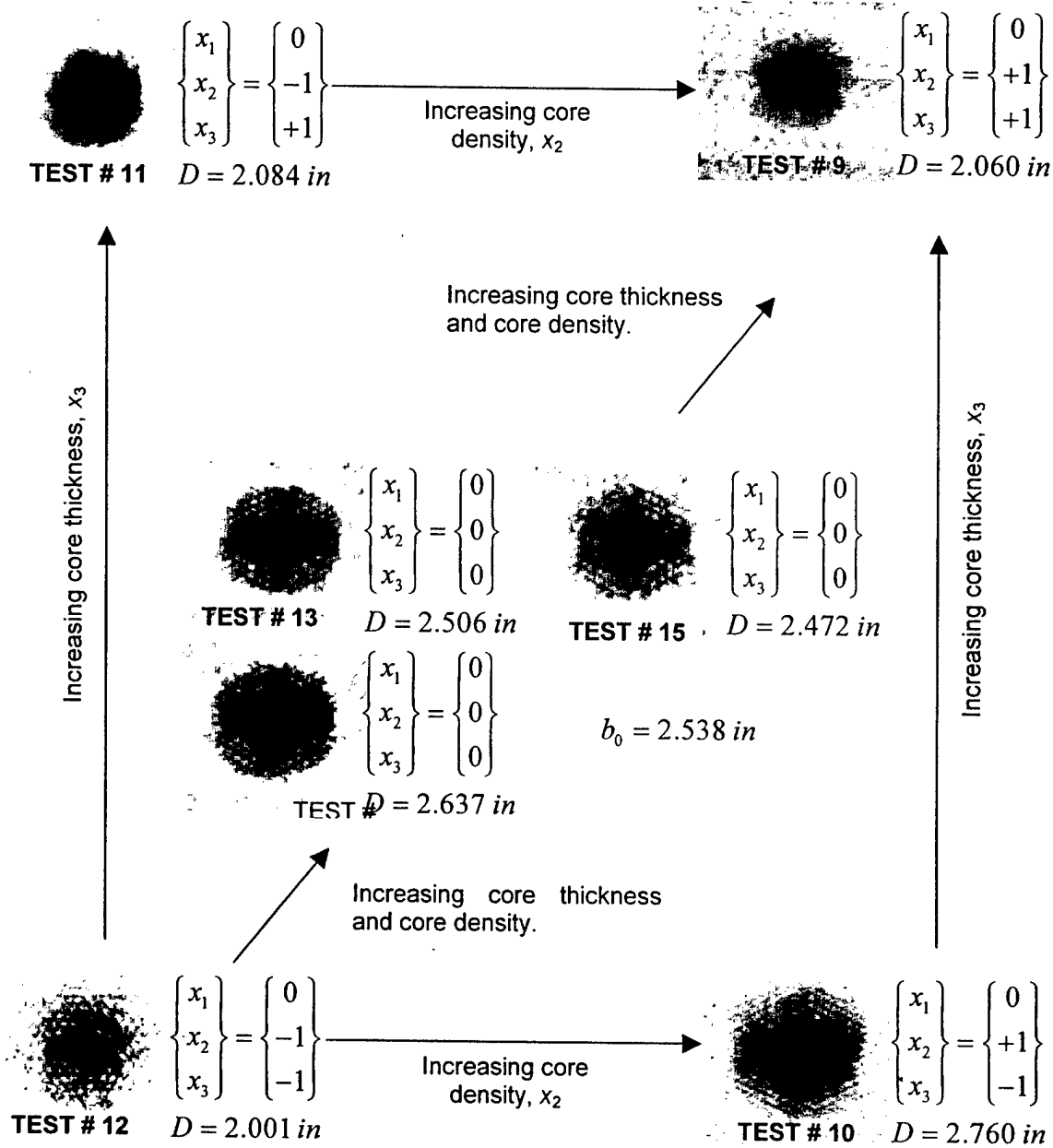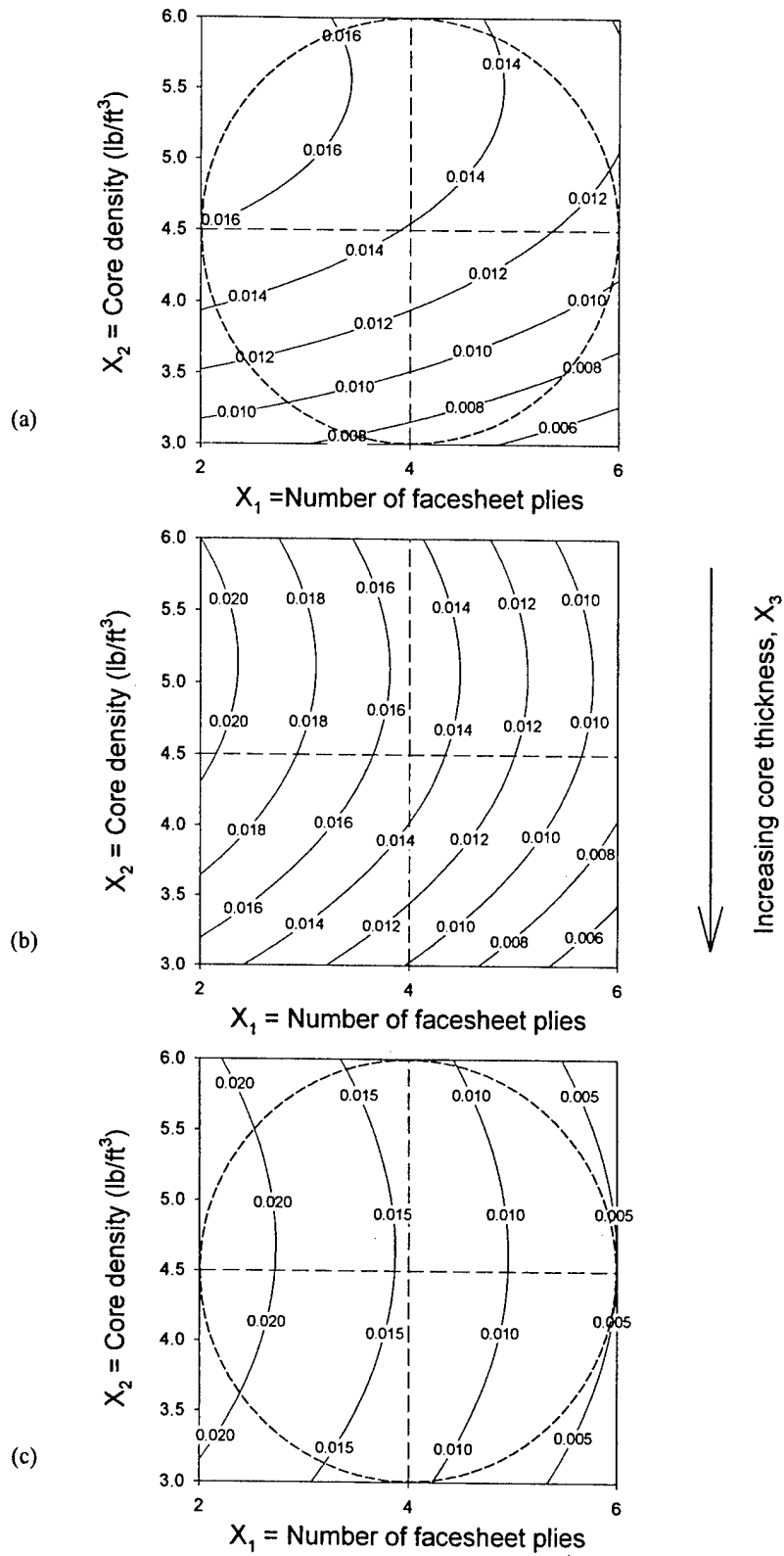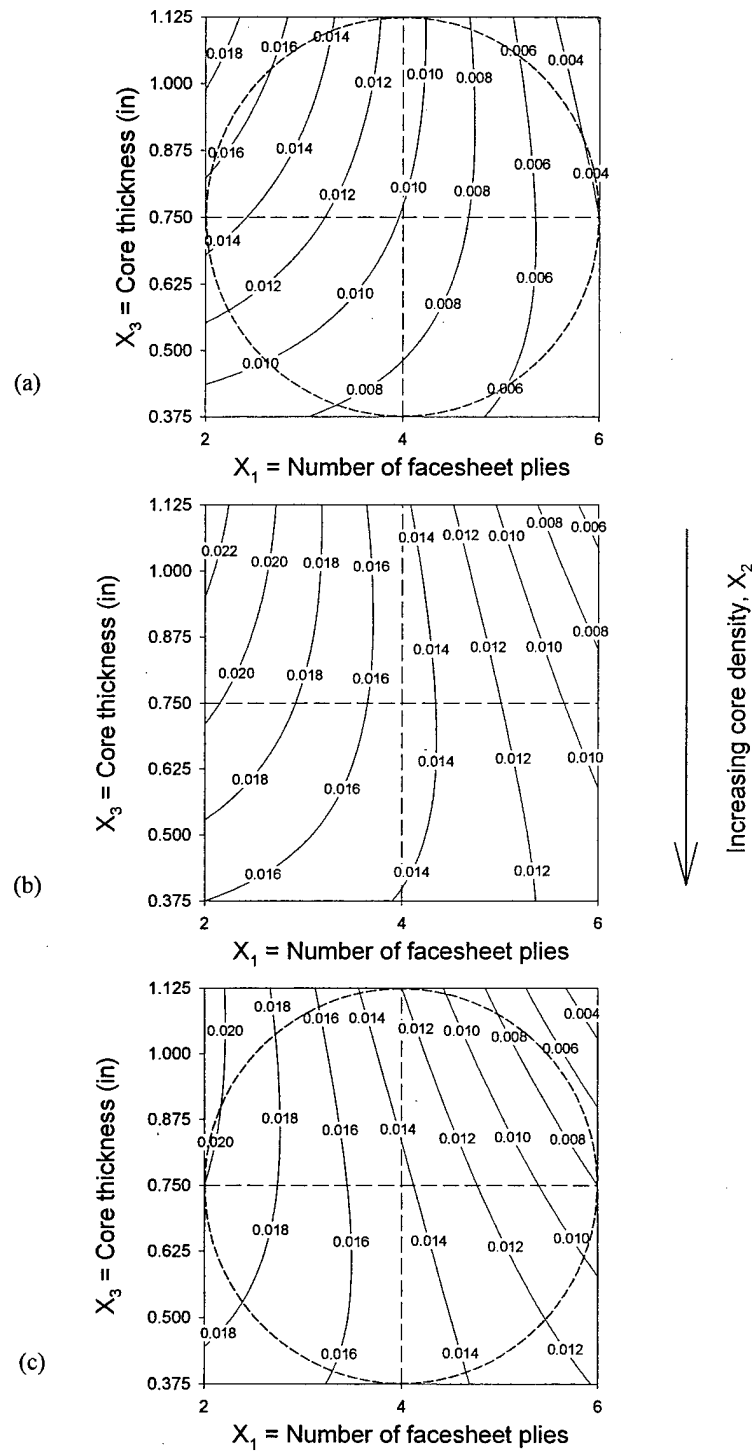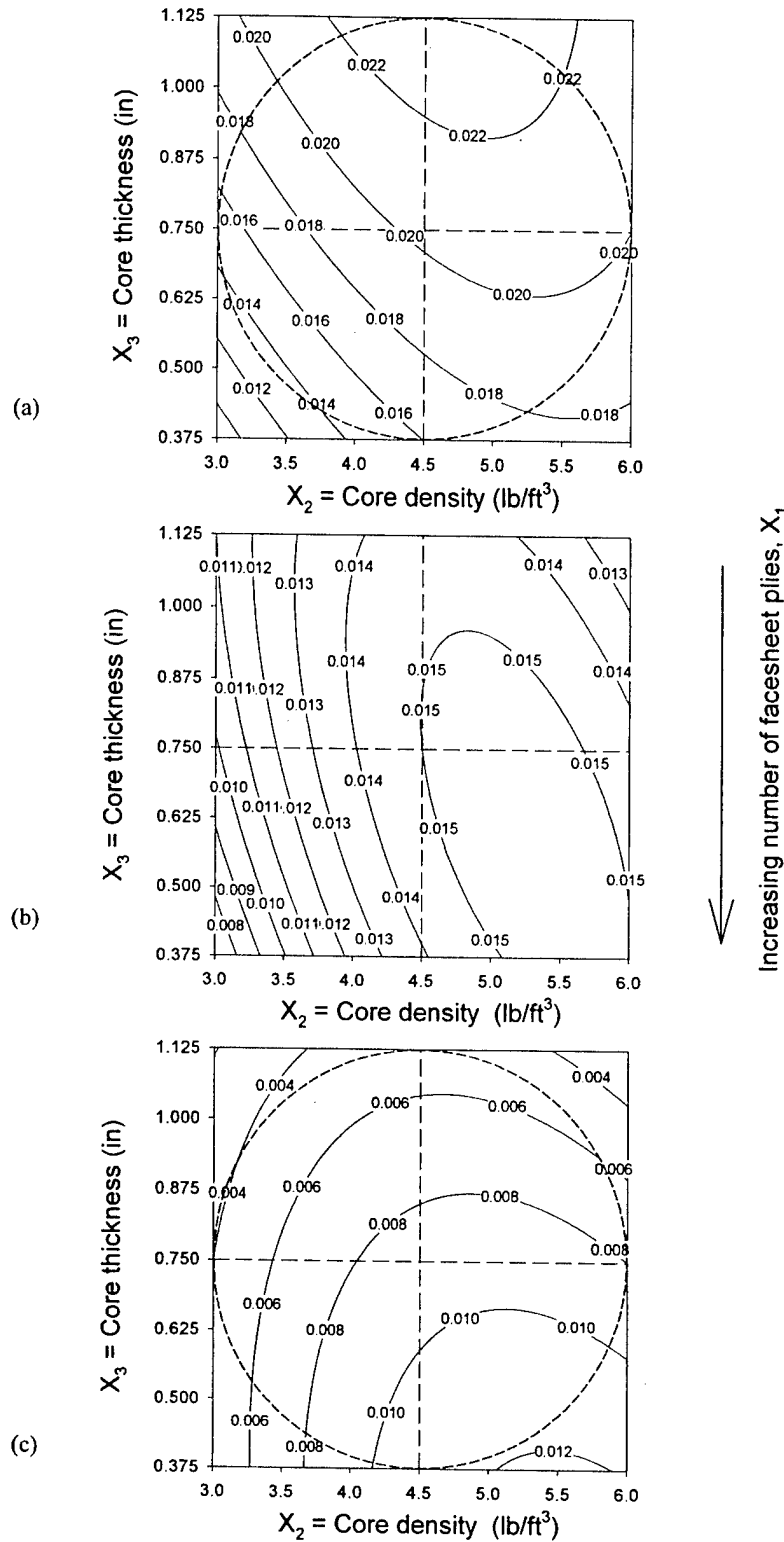
FIGURE 14. PREDICTED RESIDUAL INDENTATION DEPTH (in): (a) $X_1 = 2$ plies [90/45]$_1$; (b) $X_1 = 4$ plies [90/45]$_2$; and (c) $X_1 = 6$ plies [90/45]$_3$

The preceding regression results suggest that the response surfaces in equations 13 and 14 provide estimates of the TTU C-scan diameter and peak residual indentation depth associated with blunt object impacts that correlate reasonably well with the experimental observations that were used in developing the regression analysis. Of course, it is desirable to use the response surfaces in equations 13 and 14 to investigate the influence of other combinations of independent variables falling within the spherical domain of the response surface. Table 5 contains a limited set of additional independent experimental results from Tomblin, et al. [5], where the combination of material system variables $(X_1, X_2, X_3) = $ (4 plies, 3.0 lb/ft^3, 3/4 in) or $(x_1, x_2, x_3) = $ (0, -1, 0) lie within a coded radius, $r = \sqrt{2} = 1.414$, of the center point of the experimental design. Response surface estimates of the planar diameter of the internal damage (equation 13) and the residual facesheet indentation (equation 14) are summarized in table 5. The mean value of the experimentally measured damage diameters ($D_{mean} = 2.271$ in) for this sandwich panel configuration differed from the estimated value by 1.4% using equation 13. The difference between individual measurements and the predicted value varied between 5.0% and 21.5%, with a mean difference of 11.2%. This suggests that response surfaces similar to equation 13 may be useful tools in identifying combinations of sandwich composite material/design parameters leading to improved damage resistance properties for a given class of impact. While the mean value of the observed residual indentation depths ($d_{mean} = 0.010$ in) corresponded precisely to the estimated value using equation 14), the individual measurements deviated substantially from the predicted values in table 5. Hence, the response surface (equation 14) yields somewhat poor estimates of the individual residual indentation depths. This underscores the importance of repeatability in the experimental measurements when implementing the response methodology outlined here. It also likely suggests that the residual indentation depth is a relatively poor damage metric for the type of blunt object impacts considered in this study.

TABLE 5. INTERPOLATION OF REGRESSION RESULTS IN THE SPACE OF CODED SANDWICH CONFIGURATION VARIABLES

x_1	x_2	x_3	r	Measured Damage Diameter, D (in)	Predicted Damage Diameter, $\hat{D}$ (in)	$\left\| \dfrac{D - \hat{D}}{D} \right\|$ (%)	Measured Damage Depth, d (in)	Predicted Damage Depth, $\hat{d}$ (in)	$\left\| \dfrac{d - \hat{d}}{d} \right\|$ (%)
0	-1	0	1	2.04	2.23	9.4	0.007	0.010	41.1
0	-1	0	1	2.13	2.23	5.1	0.003	0.010	229
0	-1	0	1	2.05	2.23	8.9	0.004	0.010	146
0	-1	0	1	2.85	2.23	21.5	0.026	0.010	62.0

2.1.2 Key Observations.

In this initial part of the investigation, the coupled influence of sandwich composite material and lay-up configuration parameters on the impact damage induced was evaluated using empirically based response surfaces for sandwich composites comprised of carbon-epoxy woven fabric facesheets and Nomex honeycomb cores. A number of carefully selected tests were used to isolate the coupled influence of the number of facesheet plies, core density, and core thickness

on the damage induced in sandwich composites due to normal impact with a relatively blunt (3.0-in-diameter) spherical steel indentor; the impact energy and impact velocity were held fixed in this portion of the study. Response surface estimates of the size of the planar damage region (equation 15) show that increasing the thickness of the core material results in the greatest improvement in the damage resistance properties (i.e., the size of the planar region typically associated with core crushing is reduced). Independently increasing the number of facesheet plies and/or core density generally resulted in an increase in the size of the estimated internal damage, although simultaneously varying these parameters could result in either an improvement or degradation in the impact damage resistance properties. It seems reasonable that changes in material system parameters likely result in either enhanced or degraded penetration resistance and bending stiffness properties that govern the damage development. Response surface estimates for the maximum residual facesheet indentation (equation 16) suggest that increasing the number of facesheet plies results in the greatest decrease in the predicted surface damage. The regression results indicate that those combinations of sandwich configuration parameters leading to the maximum internal damage do not correspond to those that result in the greatest facesheet indentation. One may potentially use response surfaces similar to equations 15 and 16 in tandem to aid in sandwich composite designs that maximize the degree of detectable facesheet damage while minimizing the internal damage associated with typical impacts.

2.2 INFLUENCE OF FACESHEET THICKNESS, IMPACT ENERGY, AND IMPACTOR DIAMETER ON THE IMPACT DAMAGE RESISTANCE OF SANDWICH COMPOSITES.

In the preceding study, discussed in section 2.1, the isolated influence of sandwich parameters on the damage resistance properties of sandwich composites was investigated for a fixed set of impact parameters. In this study, the isolated effects of the number of facesheet plies (X_1), impact energy (X_4), and impactor diameter (X_5) on the damage resistance characteristics of sandwich composite panels are investigated using the Box-Behnken experimental design. Table 6 summarizes the low, midrange, and high levels of the natural (X_1, X_4, X_5) and coded (x_1, x_4, x_5) independent variables considered in this examination. Here, the core density $(X_2 = 3.0 \text{ lb/ft}^3)$, core thickness $(X_3 = 3/4 \text{ in})$, and impact velocity $(X_6 = 96.3 \text{ in/sec})$ were held fixed.

TABLE 6. NATURAL VALUES AND CORRESPONDING CODED LEVELS OF
THE SANDWICH CONFIGURATION AND IMPACT VARIABLES

i	Independent Variable	Natural Value, X_i	Coded Level, x_i
1	Number of Facesheet Plies	2 $[90/45]_1$	-1
		4 $[90/45]_2$	0
		6 $[90/45]_3$	+1
4	Impact Energy	90.0 in-lb	-1
		120 in-lb	0
		150 in-lb	+1
5	Impactor Diameter	1.0 in	-1
		2.0 in	0
		3.0 in	+1

Table 7 summarizes the combinations of coded independent variables as well as the experimentally measured damage sizes for the 15 experiments (tests 16-30) used to develop the regression analysis. Following a procedure similar to that used to develop the response surfaces described by equations 13 through 16, statistically reliable, second-order response surfaces were generated that characterize the impact damage induced as a function of the number of facesheet plies, impact energy, and impactor diameter. An estimate of the diameter of the planar damage region associated with TTU C-scan measurements from the regression analysis were expressed either in terms of coded or natural values of the independent variables, i.e.,

$$\hat{D} = 2.057 + 0.3773 \cdot x_1 + 0.3234 \cdot x_4 + 0.3506 \cdot x_5$$
$$\ldots + 0.08412 \cdot x_1^2 - 0.1456 \cdot x_4^2 + 0.1084 \cdot x_5^2 \qquad \text{(in)} \qquad \text{(17a)}$$
$$\ldots + 0.4400 \cdot x_1 \cdot x_4 + 0.1280 \cdot x_1 \cdot x_5 + 0.3308 \cdot x_4 \cdot x_5$$

and

$$\hat{D} = 4.426 - 0.9876 \cdot X_1 - 1.771 \cdot 10^{-3} \cdot X_4 - 1.662 \cdot X_5$$
$$\ldots + 0.02103 \cdot X_1^2 - 1.618 \cdot 10^{-4} \cdot X_4^2 + 0.1084 \cdot X_5^2 \qquad \text{(in)} \qquad \text{(17b)}$$
$$\ldots + 7.333 \cdot 10^{-3} \cdot X_1 \cdot X_4 + 0.06400 \cdot X_1 \cdot X_5 + 0.01103 \cdot X_4 \cdot X_5$$

TABLE 7. COMPARISONS BETWEEN PREDICTED AND MEASURED DAMAGE SIZES
(From tests 16 to 30)

Test, k	x_1	x_4	x_5	Measured Damage Diameter, D (in)	Predicted Damage Diameter, $\hat{D}$ (in)	$\left\lvert \dfrac{D - \hat{D}}{D} \right\rvert$ (%)	Measured Damage Depth, d (in)	Predicted Damage Depth, $\hat{d}$ (in)	$\left\lvert \dfrac{d - \hat{d}}{d} \right\rvert$ (%)
16	+1	+1	0	3.12	3.13	0.2	0.01	0.002	83.9
17	+1	-1	0	1.75	1.60	8.1	0.007	-0.01	360
18	-1	+1	0	1.36	1.50	10.4	0.12	0.14	20.7
19	-1	-1	0	1.74	1.73	0.4	0.07	0.08	15.3
20	+1	0	+1	2.87	3.10	8.1	0.006	0.04	700
21	+1	0	-1	2.24	2.14	4.4	0.03	0.03	13.5
22	-1	0	+1	1.99	2.09	5.0	0.01	0.01	35.7
23	-1	0	-1	1.88	1.65	12.4	0.35	0.31	11.8
24	0	+1	+1	3.26	3.02	7.4	0.009	-0.02	336
25	0	+1	-1	1.57	1.66	5.8	0.15	0.16	11.2
26	0	-1	+1	1.80	1.71	5.1	0.005	-0.01	335
27	0	-1	-1	1.43	1.67	16.7	0.04	0.07	63.0
28	0	0	0	2.13	2.05	3.4	0.03	0.02	28.8
29	0	0	0	2.09	2.05	2.0	0.02	0.02	5.3
30	0	0	0	1.94	2.05	5.9	0.01	0.02	54.9

The constant term (b_0 = 2.05 in) in equation 17a represents the mean diameter of the TTU C-scan image for those panels corresponding to the center point of the design. Note that based upon the magnitudes of the coefficients of the linear terms in equation 17a, the coded number of facesheet plies, x_1, impact energy, x_4, and impactor diameter, x_5, contribute almost equally to the linear variation in the predicted response at points removed from the center point $(x_1, x_4, x_5) = (0, 0, 0)$ of the designed test matrix (e.g., increasing/decreasing any of the independent variables from its midrange value will result in a linear increase/decrease in the predicted damage diameter from b_0). It makes sense that increasing either the impact energy or the impactor diameter will produce internal damage that is spread over a greater area. Following the arguments made previously, an increase in the penetration resistance (i.e., increasing the number of facesheet plies) will likely also result in more distributed damage. Similar arguments can be made when interpreting the influence of the remaining quadratic and coupling terms in equation 17a on the predicted response.

Analogously, an estimate of the maximum residual facesheet indentation from the regression analysis may be expressed either in terms of coded or natural values of the independent variables, i.e.,

$$\hat{d} = \left[26.33 - 63.00 \cdot x_1 + 19.75 \cdot x_4 - 69.95 \cdot x_5 \right.$$
$$... + 39.33 \cdot x_1^2 - 10.67 \cdot x_4^2 + 37.33 \cdot x_5^2 \qquad \text{(in)} \qquad (18a)$$
$$\left. ... - 9.500 \cdot x_1 \cdot x_4 + 77.50 \cdot x_1 \cdot x_5 - 24.50 \cdot x_4 \cdot x_5 \right] \cdot 10^{-3}$$

and

$$\hat{d} = \left[386.3 - 168.7 \cdot X_1 + 5.769 \cdot X_4 - 275.8 \cdot X_5 \right.$$
$$... + 9.833 \cdot X_1^2 - 0.01185 \cdot X_4^2 + 37.33 \cdot X_5^2 \qquad \text{(in)} \qquad (18b)$$
$$\left. ... - 0.1583 \cdot X_1 \cdot X_4 + 38.75 \cdot X_1 \cdot X_5 - 0.8167 \cdot X_4 \cdot X_5 \right] \cdot 10^{-3}$$

The constant term (b_0 = 0.02 in) in equation 18a represents the mean value of the peak residual facesheet indentation for the three center runs. As might be expected, the magnitudes of the coefficients of the linear terms in equation 18a suggest an increase in the number of facesheet plies, x_1, or impactor diameter, x_5, will result in a linear decrease in the predicted response at points removed from the center point of the test matrix while an increase in the impact energy, x_4, will tend to produce a linear increase in the predicted response. Analogous arguments can be made when interpreting the influence of the remaining terms in equation 18a on the estimated response.

2.2.1 Discussion of Facesheet Configuration and Impact Parameter Regression Model Results.

Table 7 also summarizes the measured and predicted planar damage diameter and the maximum residual facesheet indentation for each of the sandwich composite panels considered in this effort. The difference between the experimentally measured damage diameters and the estimated values using equation 17 varied between 0.2% and 16.7% for the 15 panels tested, with a mean difference of 6.4%. This suggests that the response surface (equation 17) provides a reasonable

characterization of the influence of the number facesheet plies, impact energy, and impactor diameter on the planar size of the internal damage generated due to impact. The regression results may also be viewed schematically in the space of coded independent variables as shown in figure 15.
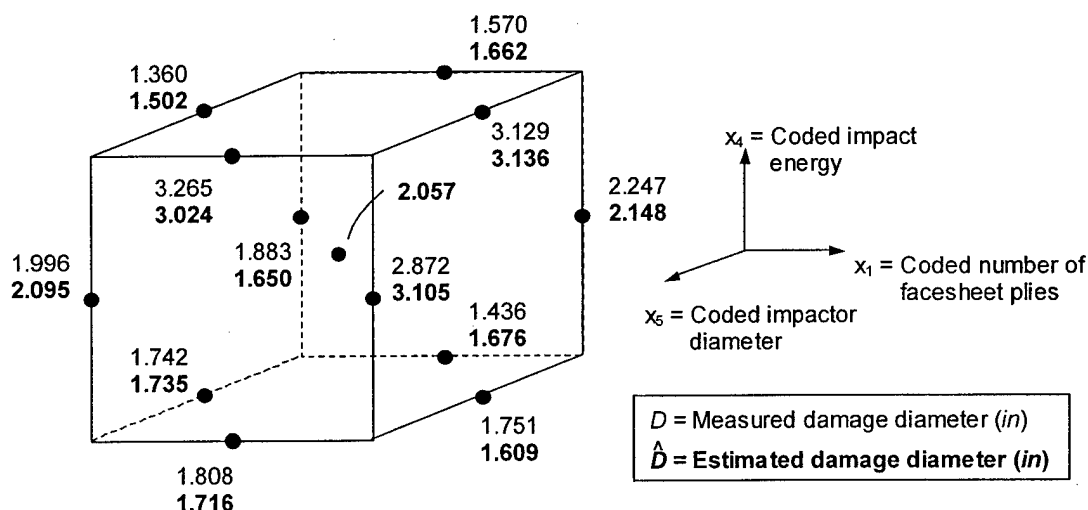
FIGURE 15. RESPONSE SURFACE ESTIMATES OF THE INTERNAL DAMAGE
DIAMETER AS A FUNCTION OF SANDWICH CONFIGURATION AND
IMPACT PARAMETERS

For the impactor diameters (1.0-3.0 in diameter) considered here, the experimentally measured peak residual facesheet indentation ranged from values on the order of the ply thickness to values representing a significant fraction of the sandwich panel stack-up thickness (d = 0.005-0.35 in; core thickness, X_3 = 3/4 in). While the magnitudes of the differences between the measured and predicted indentation depths were all within 1/20 in, the percentage difference between the two values was unacceptably large, particularly for those test configurations leading to relatively shallow indentations (e.g., those tests involving 6-ply facesheets and/or a 3.0-in-diameter impactor). Several of the latter test configurations resulted in negative response surface estimates of the peak residual facesheet indentation (i.e., facesheet bulging). These disparities are attributable to (1) the relatively large scatter in the center point residual facesheet indentation measurements used to determine the constant, b_0, in equation 18a and (2) the two orders of magnitude difference between the extremes values in the residual indentation measurements (d_{max} = 0.35 in, d_{min} = 0.005 in). Hence, the minimum values of the measured residual facesheet indentation are relatively close to zero (as well as to the limits of mechanical measurement) in comparison to the maximum value over the range of test parameters. Future efforts associated with this work will examine possible normalization of the residual facesheet indentation data in order to address this issue. Note that for those combinations of test parameters leading to higher levels of facesheet damage (e.g., those tests involving 2-ply facesheets and/or a 1.0-in-diameter impactor), the correlation between the experimental and regression results is somewhat improved. Similar to section 2.1, the response surface estimate of the peak indentation depth (equation 18) is likely inaccurate for the class of blunt object impacts considered here, particularly for the case of extremely shallow indentation profiles. Qualitative consideration of

the response surface (equation 18), however, may prove useful in identifying key combinations of material system and impact parameters that lead to the greatest degree of visibly detectable damage.

Figures 16 through 21 summarize the influence of the number of facesheet plies (X_1, x_1), impact energy (X_4, x_4), and impactor diameter (X_5, x_5) on the size of the planar damage region. Figures 16(a), 16(b), and 16(c) show the predicted damage diameter (equation 17) as a function of facesheet thickness and impact energy for impactor diameter values of X_5 = 1.0, 2.0, and 3.0 in (or x_5 = -1, 0, 1), respectively. It is clear from figures 16(a) through 16(c), that the peak planar damage diameter is generally an increasing function of the number of facesheet plies, impact energy, and impactor diameter. Based upon the regression analysis, the maximum planar damage dimension for a given impactor diameter occurs where the number of facesheet plies and impact energy are evaluated at their high levels; the peak damage diameter occurs where all three independent variables are evaluated at their high levels (see figure 16(c)). Given the enhanced penetration resistance associated with the 6-ply facesheet configuration, it seems reasonable that the maximum internal damage would occur for maximum energy impacts involving a relatively blunt 3.0-in-diameter indentor. Note, from figure 16(b), the an increase in the impact energy for the 2-ply facesheet configuration from 90 in-lb to 150 in-lb results in a decrease in the estimated damage diameter; the development of more localized damage is likely a consequence of facesheet penetration occurring at the higher impact energy levels. These results are in agreement with the experimental observations. Figure 17 shows the TTU C-scan images and recorded damage diameters for the test configurations involving the midrange impactor diameter (x_5 = 0; X_5 = 2.0 in). Consistent with the regressions of figure 16(b), the recorded damage diameter was a maximum where (x_1, x_4, x_5) = (1, 1, 0) or (X_1, X_4, X_5) = (6 plies, 150 in-lb, 2.0 in), and a relative minimum where facesheet penetration is most likely to occur, i.e., (x_1, x_4, x_5) = (-1, 1, 0) or (X_1, X_4, X_5) = (2 plies, 150 in-lb, 2.0 in). As mentioned previously, there is likely a competition between enhanced penetration resistance and improved bending stiffness associated with changes in material variables that govern the damage development.

Figures 18(a), 18(b), and 18(c) show the predicted damage diameter (equation 17) as a function of the number of facesheet plies and impactor diameter for impact energy values of X_4 = 90.0, 120, and 150 in-lb or (x_4 = -1, 0, 1), respectively. Similar to the preceding case, the impact damage based upon the regression analysis is generally an increasing function of both the number of facesheet plies and impactor diameter, particularly at midrange to high impact energy levels. Note that increasing the impactor diameter from 1.0 in to 3.0 in can result in a significant increase in the size of the internal damage. This underscores the need to consider a variety of impactor diameters when establishing a damage tolerance plan for sandwich composite aircraft structures. Figure 19 shows the TTU C-scan images and recorded damage diameters for test configurations corresponding to the midrange impact energy level (x_4 = 0; X_4 = 120 in-lb). Consistent with the regression of figure 18(b), the recorded damage diameters increased sharply as the number of facesheet plies and impactor diameter were simultaneously increased from low to high values.
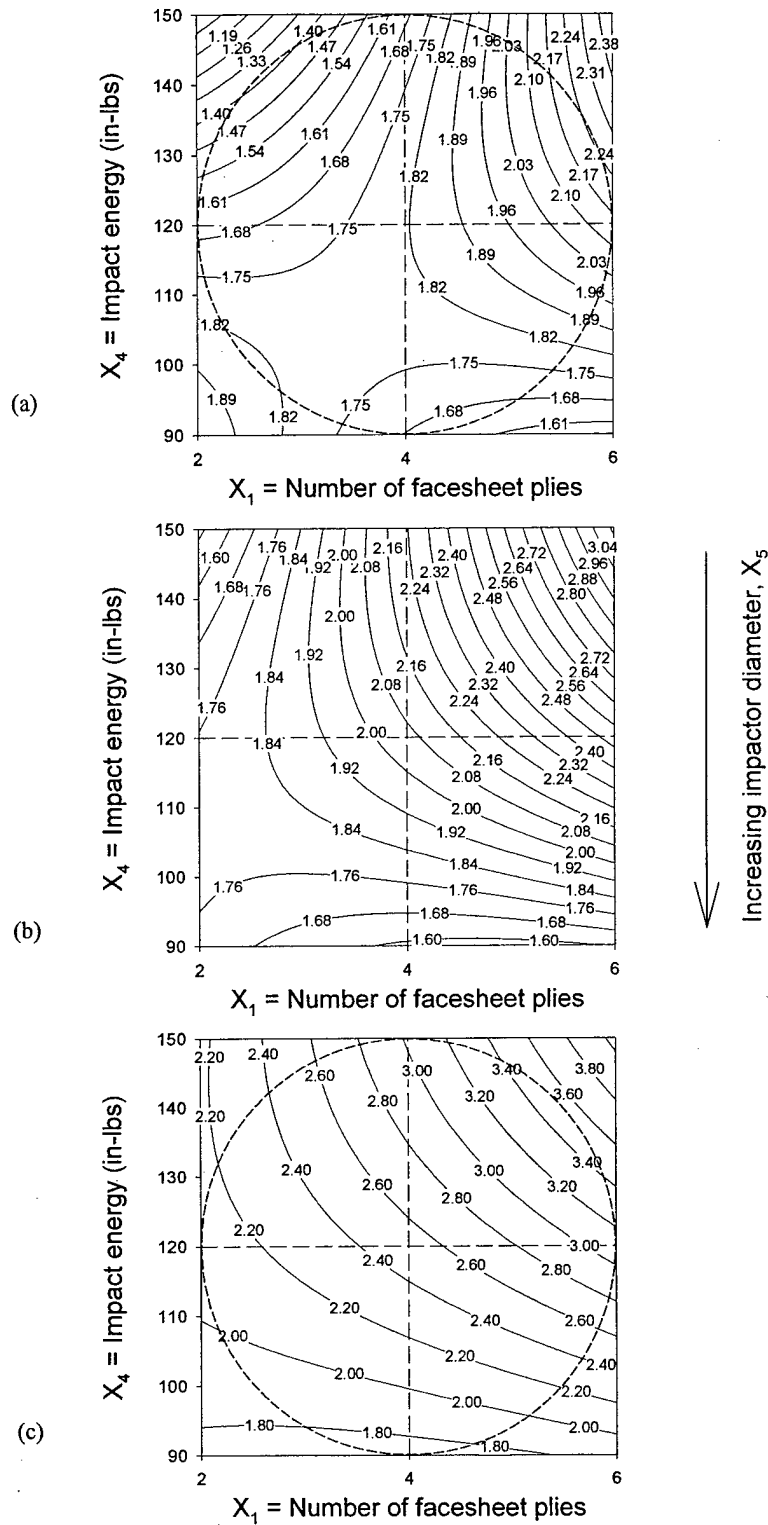
FIGURE 16. PREDICTED DAMAGE DIAMETER (in): (a) $X_5 = 1.0$ in; (b) $X_5 = 2.0$ in; and (c) $X_5 = 3.0$ in
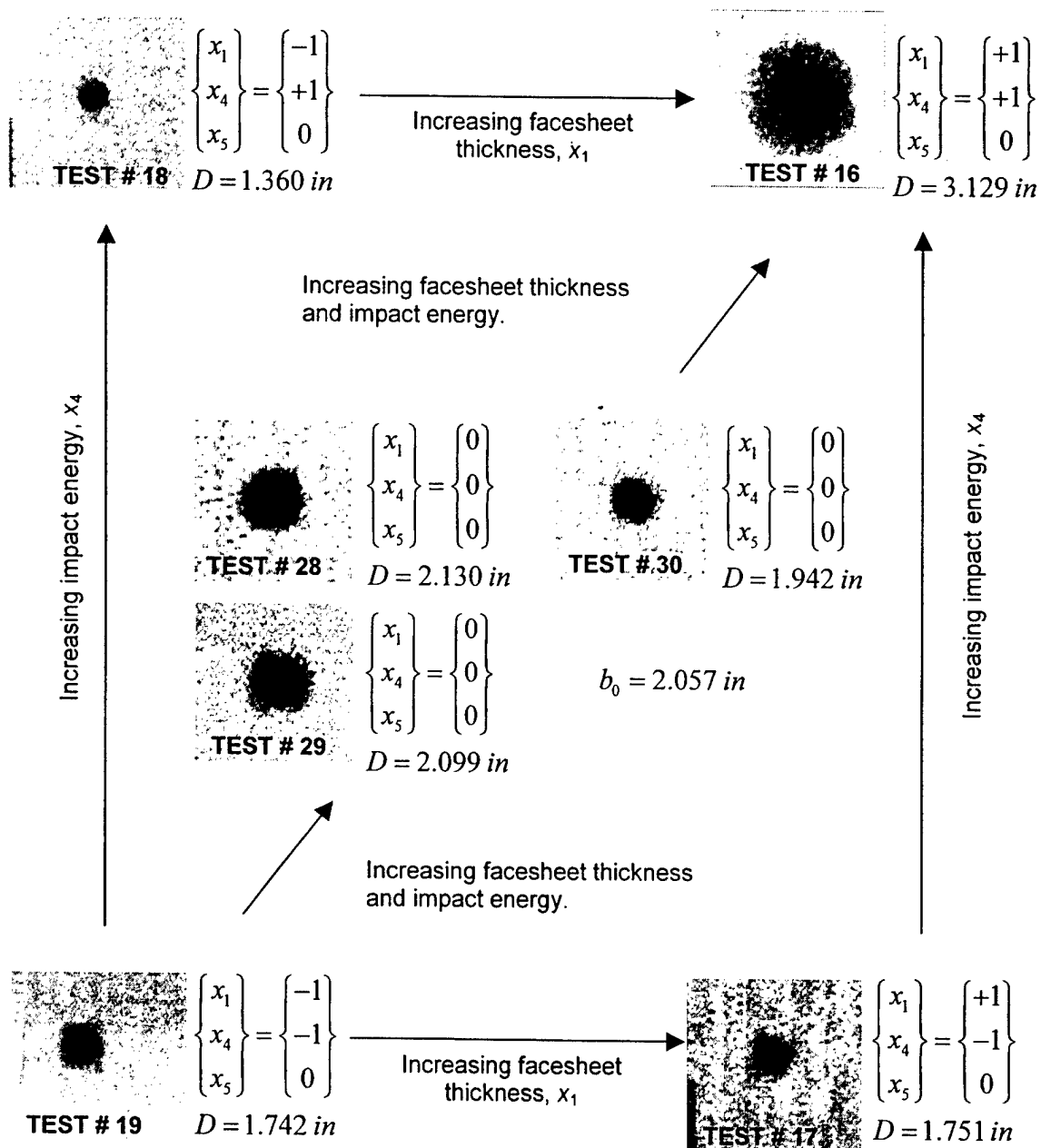
FIGURE 17. MEASURED DAMAGE DIAMETER FOR IMPACTOR
DIAMETER, $X_5 = 2.0$ in ($x_5 = 0$)
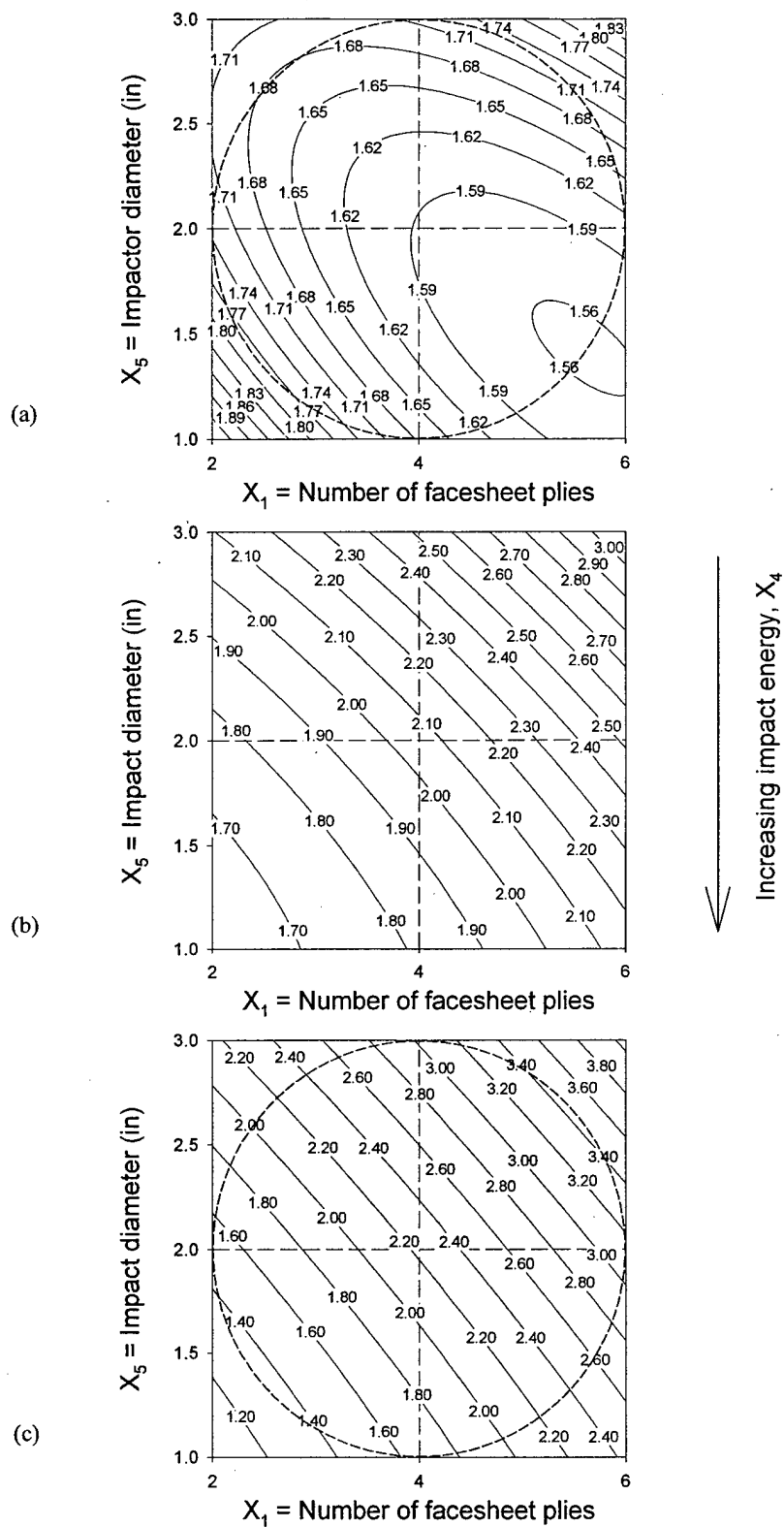
FIGURE 18. PREDICTED DAMAGE DIAMETER (in): (a) X_4 = 90.0 in-lb; (b) X_4 = 120 in-lb; and (c) X_4 = 150 in-lb

33

TEST # 22 $D = 1.996\,in$

$$\begin{Bmatrix} x_1 \\ x_4 \\ x_5 \end{Bmatrix} = \begin{Bmatrix} -1 \\ 0 \\ +1 \end{Bmatrix}$$

Increasing facesheet thickness, x_1

TEST # 20 $D = 2.872\,in$

$$\begin{Bmatrix} x_1 \\ x_4 \\ x_5 \end{Bmatrix} = \begin{Bmatrix} +1 \\ 0 \\ +1 \end{Bmatrix}$$

Increasing impactor diameter, x_5

Increasing facesheet thickness and impactor diameter.

TEST # 28 $D = 2.130\,in$

$$\begin{Bmatrix} x_1 \\ x_4 \\ x_5 \end{Bmatrix} = \begin{Bmatrix} 0 \\ 0 \\ 0 \end{Bmatrix}$$

TEST # 30 $D = 1.942\,in$

$$\begin{Bmatrix} x_1 \\ x_4 \\ x_5 \end{Bmatrix} = \begin{Bmatrix} 0 \\ 0 \\ 0 \end{Bmatrix}$$

Increasing impactor diameter,

TEST # 29 $D = 2.099\,in$

$$\begin{Bmatrix} x_1 \\ x_4 \\ x_5 \end{Bmatrix} = \begin{Bmatrix} 0 \\ 0 \\ 0 \end{Bmatrix}$$

$b_0 = 2.057\,in$

Increasing facesheet thickness and impactor diameter.

TEST # 23 $D = 1.883\,in$

$$\begin{Bmatrix} x_1 \\ x_4 \\ x_5 \end{Bmatrix} = \begin{Bmatrix} -1 \\ 0 \\ -1 \end{Bmatrix}$$

Increasing facesheet thickness, x_1

TEST # 21 $D = 2.247\,in$

$$\begin{Bmatrix} x_1 \\ x_4 \\ x_5 \end{Bmatrix} = \begin{Bmatrix} +1 \\ 0 \\ -1 \end{Bmatrix}$$

FIGURE 19. MEASURED DAMAGE DIAMETER FOR IMPACT ENERGY,
$X_4 = 120$ in-lb ($x_4 = 0$)

Figures 20(a), 20(b), and 20(c) show the predicted damage diameter (equation 17) as a function of impact energy and impactor diameter for the 2-, 4-, and 6-ply facesheet configurations, respectively. Again, the estimated impact damage is generally an increasing function of the impact energy and impactor diameter, particularly for the 4- and 6-ply facesheet configurations. Note that for sandwich panels comprised of 2-ply facesheets impacted with low- to midrange impactor diameters (figure 20(a)), an increase in the impact energy can result in a decrease in the predicted planar damage dimension that may be associated with more localized facesheet damage/penetration. Figure 21 shows the TTU C-scan images and recorded damage diameters for test configurations corresponding to the midrange facesheet configuration ($x_1 = 0$; $X_1 = 4$ plies) that are consistent with the regression of figure 20(b).
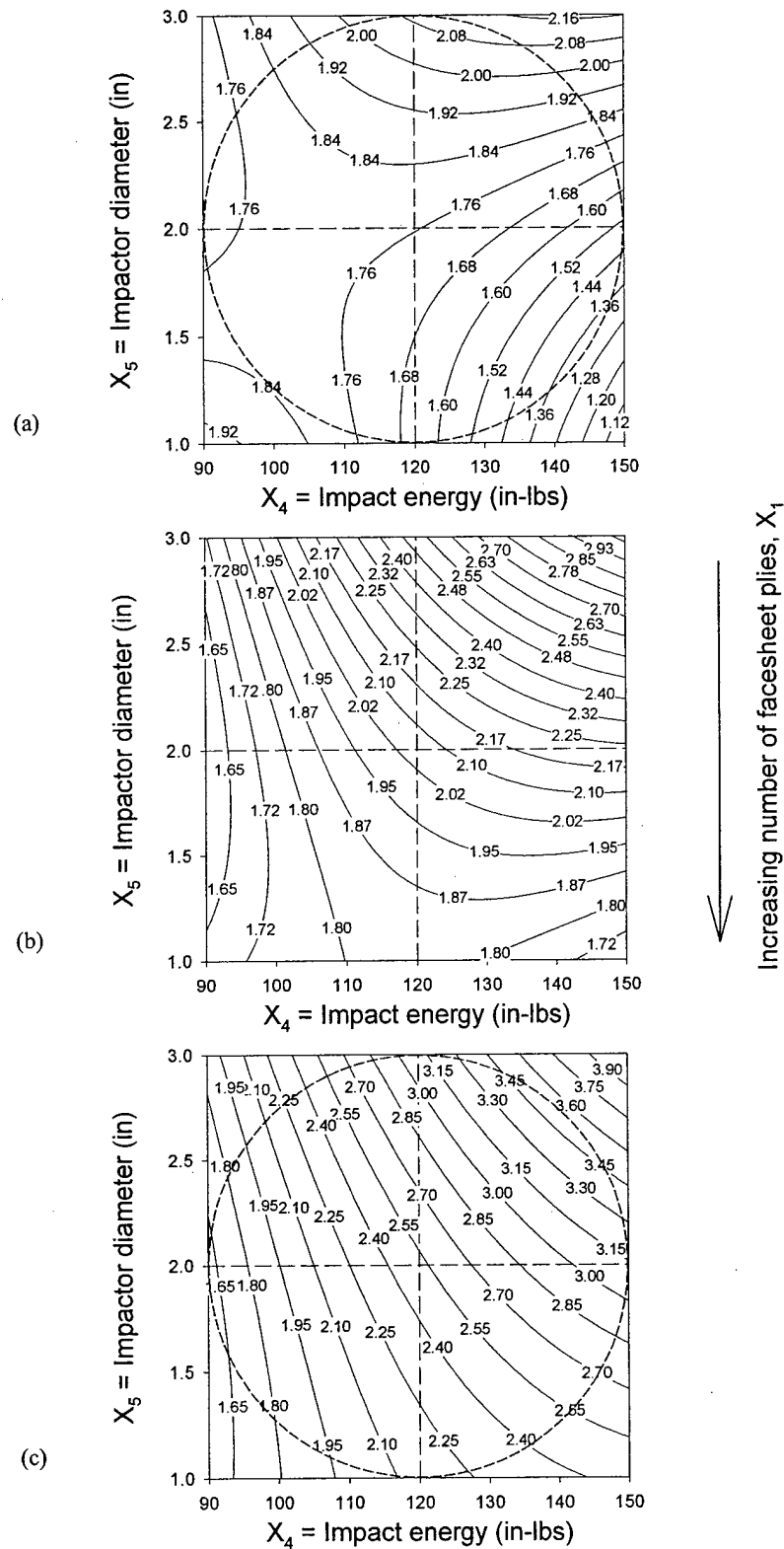
FIGURE 20. PREDICTED DAMAGE DIAMETER (in): (a) $X_1 = 2$ plies $[90/45]_1$;
(b) $X_1 = 4$ plies $[90/45]_2$, and (c) $X_1 = 6$ plies $[90/45]_3$

35

Increasing impact energy, x_4

$\begin{Bmatrix} x_1 \\ x_4 \\ x_5 \end{Bmatrix} = \begin{Bmatrix} 0 \\ -1 \\ +1 \end{Bmatrix}$

TEST # 26 $D = 1.808\ in$

$\begin{Bmatrix} x_1 \\ x_4 \\ x_5 \end{Bmatrix} = \begin{Bmatrix} 0 \\ +1 \\ +1 \end{Bmatrix}$

TEST # 24 $D = 3.265\ in$

Increasing impact energy and impactor diameter.

Increasing impactor diameter, x_5

$\begin{Bmatrix} x_1 \\ x_4 \\ x_5 \end{Bmatrix} = \begin{Bmatrix} 0 \\ 0 \\ 0 \end{Bmatrix}$

TEST # 28 $D = 2.130\ in$

$\begin{Bmatrix} x_1 \\ x_4 \\ x_5 \end{Bmatrix} = \begin{Bmatrix} 0 \\ 0 \\ 0 \end{Bmatrix}$

TEST # 30 $D = 1.942\ in$

$\begin{Bmatrix} x_1 \\ x_4 \\ x_5 \end{Bmatrix} = \begin{Bmatrix} 0 \\ 0 \\ 0 \end{Bmatrix}$

TEST # 29 $D = 2.099\ in$

$b_0 = 2.057\ in$

Increasing impactor diameter, x_5

Increasing impact energy and impactor diameter.

$\begin{Bmatrix} x_1 \\ x_4 \\ x_5 \end{Bmatrix} = \begin{Bmatrix} 0 \\ -1 \\ -1 \end{Bmatrix}$

TEST # 27 $D = 1.436\ in$

Increasing impact energy, x_4

$\begin{Bmatrix} x_1 \\ x_4 \\ x_5 \end{Bmatrix} = \begin{Bmatrix} 0 \\ +1 \\ -1 \end{Bmatrix}$

TEST # 25 $D = 1.570\ in$

FIGURE 21. MEASURED DAMAGE DIAMETER FOR FACESHEET CONFIGURATION, $X_1 = 4$ plies [90/45]$_2$ ($x_1 = 0$)

Figures 22 through 24 summarize the influence of the number of facesheet plies, impact energy, and impactor diameter on the maximum residual facesheet indentation. While it is recognized that using the response surface (equation 18) is likely inappropriate to estimate particularly shallow residual facesheet indentations associated with the 3.0-in-diameter impactor, it may be helpful in identifying those combinations of material and impact parameters that lead to the maximum (i.e., most visible) surface damage. Figures 22, 23, and 24 each contain three

response surface contour plots for the cases where the impactor diameter, impact energy, and number of facesheet plies are varied between low, midrange, and high values. In each set of figures, the peak residual facesheet indentation typically occurs where the number of facesheet plies and impactor diameter are minimized and where the impact energy is maximized. This is consistent with the experimental observations (see table 7). More importantly, a critical comparison of figures 16, 18, and 20 to figures 22, 23, and 24 suggests that those combinations of sandwich configuration and impact parameters that lead to the maximum amount of internal damage (and possibly the greatest relative reduction in residual strength [5]) do not correspond to the configurations that produce the greatest facesheet indentation (i.e., damage configurations that are amenable to visual inspection).

Table 8 contains a set of additional independent experimental results from Tomblin, et al. [5], where the ranges of coded material system and impact variables are in the vicinity of those considered in this study. Response surface estimates of the planar diameter of the internal damage (equation 17) and the residual facesheet indentation (equation 18) are summarized in table 8. Note that the combinations of the coded number of facesheet plies (x_1), impact energy (x_4), and impactor diameter (x_5) contained in the first eight rows of the table lie within a coded radius, $r = \sqrt{2} = 1.414$, of the center point of the experimental design; interpolation of response surface results is appropriate for these data. The remaining combinations of independent variables, however, all correspond to $r > \sqrt{2}$. Use of the response surfaces (equations 17 and 18) for the latter case corresponds to an extrapolation beyond the range of independent variables used in the regression; such estimates are denoted in the table by an asterisk (*).

The difference between the experimentally measured damage diameters and the interpolated values varied between 4.4% and 24.2%, with a mean difference of 14.6%. Hence, the response surface estimates using equation 16 correlate moderately well with the experimental data within the space of the Box-Behnken design. The first three extrapolated values of the planar damage diameter contained in the table correspond combinations of independent variables that fall just outside of the coded radius, $r = \sqrt{2}$; the response surface (equation 17) correlates reasonably well with the experimental data for these cases. The remaining combinations of independent variables, however, correspond to extrapolation of regression results toward various corners of the cube shown in figure 15 (i.e., $r = \sqrt{x_1^2 + x_4^2 + x_5^2} \approx \sqrt{3} = 1.732$). As can be seen from table 8, the magnitudes of the differences between the measured and extrapolated values of the damage diameter are, in general, significantly larger than for the case involving interpolation of results. The maximum difference between the measured and extrapolated results (71%) occurred for (x_1, x_4, x_5) = (1, 0.78, 1) or (X_1, X_4, X_5) = (6 plies, 143 in-lb, 3.0 in). As can be seen in figure 20(c), there exists a relatively large gradient in the extrapolated response surface prediction along the radial line defined by the points (X_1, X_4, X_5) = (6 plies, 120 in-lb, 2.0 in) and (X_1, X_4, X_5) = (6 plies, 150 in-lb, 3.0 in). Clearly, extreme caution must be used to ensure that response surfaces estimates are only evaluated in the spherical domain associated with the experimental design (in this case, $r \leq \sqrt{2}$).

FIGURE 22. PREDICTED RESIDUAL INDENTATION DEPTH (in): (a) $X_5 = 1.0$ in; b) $X_5 = 2.0$ in; and (c) $X_5 = 3.0$ in

FIGURE 23. PREDICTED RESIDUAL INDENTATION DEPTH (in): (a) $X_4 = 90.0$ in-lb; (b) $X_4 = 120$ in-lb; and (c) $X_4 = 150$ in-lb

FIGURE 24. PREDICTED RESIDUAL INDENTATION DEPTH (in): (a) X_1 = 2 plies $[90/45]_1$; (b) X_1 = 4 plies $[90/45]_2$; and (c) X_1 = 6 plies $[90/45]_3$
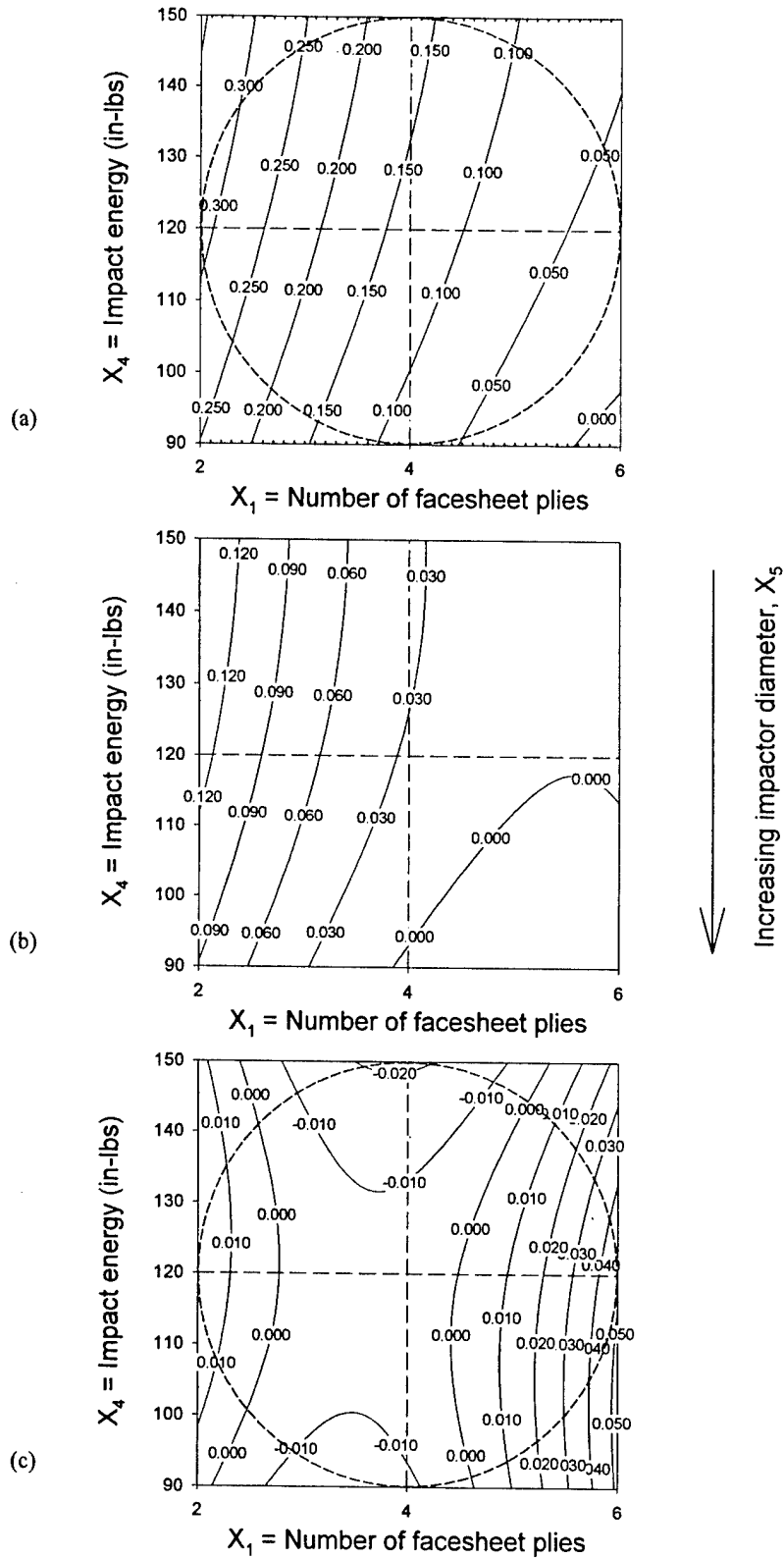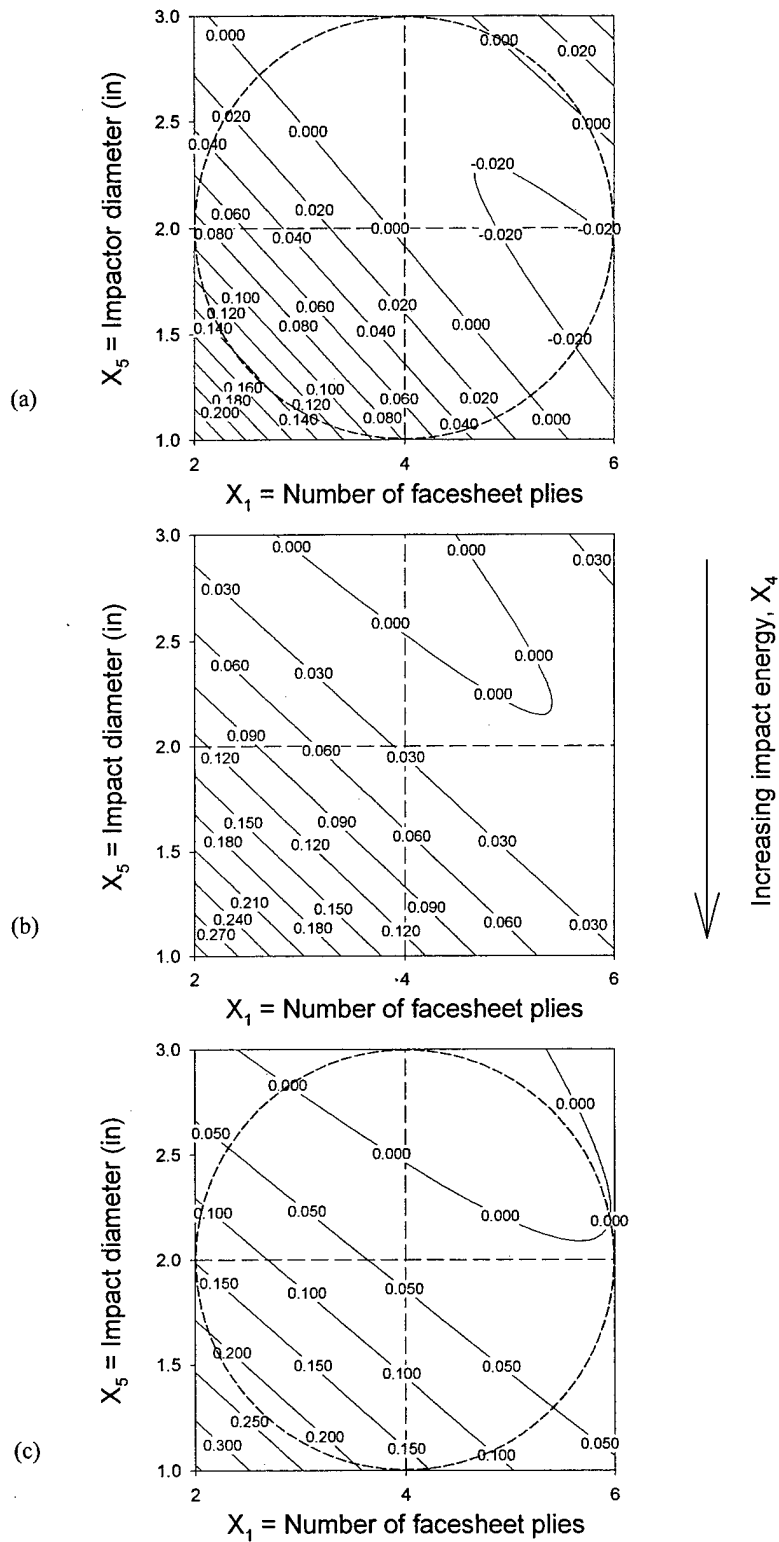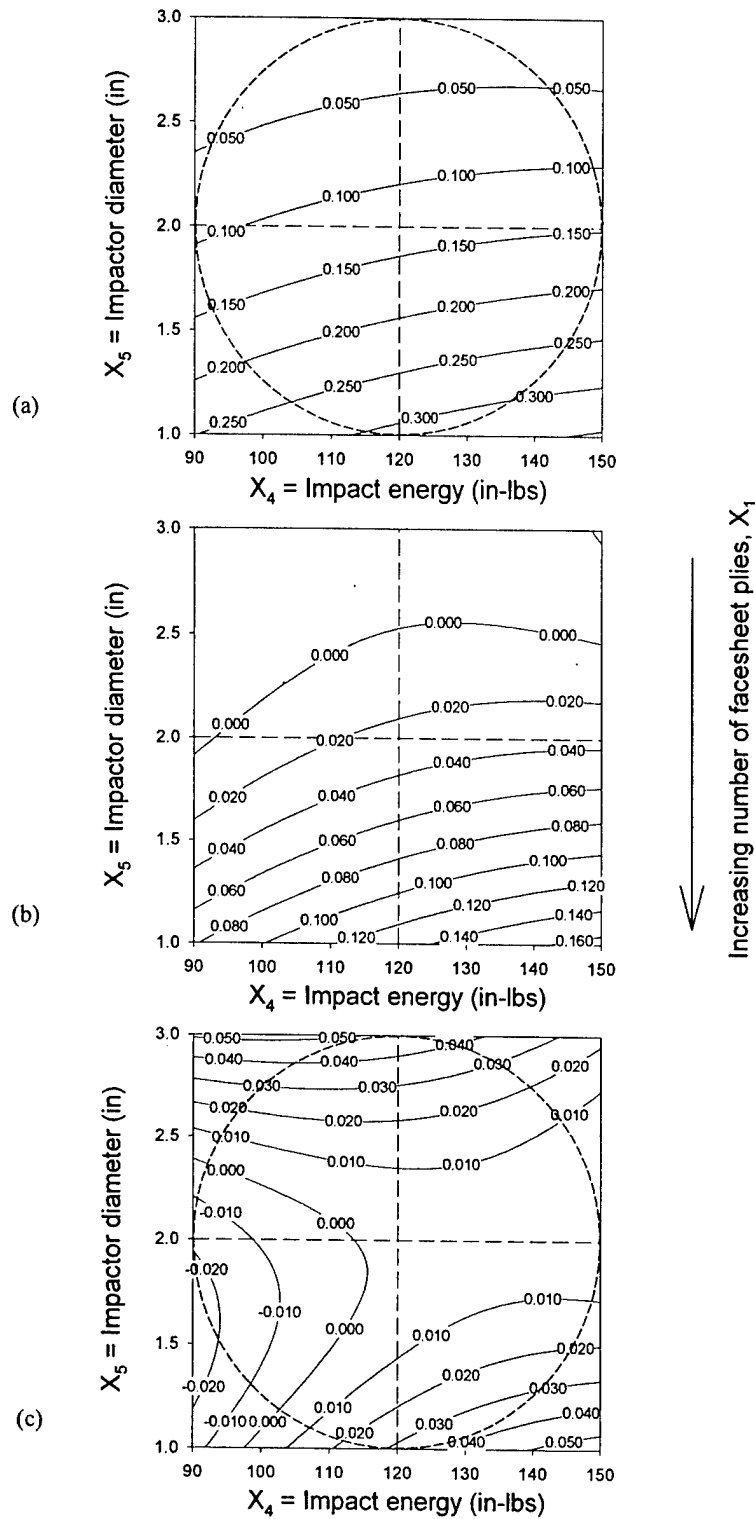
TABLE 8. INTERPOLATION/EXTRAPOLATION OF REGRESSION RESULTS IN THE SPACE OF CODED SANDWICH CONFIGURATION AND IMPACT VARIABLES

x_1	x_4	x_5	r	Measured Damage Diameter, D (in)	Predicted Damage Diameter, $\hat{D}$ (in)	$\left\|\dfrac{D-\hat{D}}{D}\right\|$ (%)	Measured Damage Depth, d (in)	Predicted Damage Depth, $\hat{d}$ (in)	$\left\|\dfrac{d-\hat{d}}{d}\right\|$ (%)
0	0.03	-1	1.0	1.89	1.81	4.4	0.13	0.13	2.5
0	0.04	1	1.0	2.04	2.54	24.2	0.007	-0.006	186
0	0.04	1	1.0	2.13	2.54	19.3	0.003	-0.006	301
0	0.05	1	1.0	2.05	2.55	23.9	0.004	-0.006	252
0	0.28	-1	1.03	1.64	1.80	9.8	0.11	0.14	24.8
0	0.30	1	1.04	2.85	2.69	5.3	0.02	-0.008	131
0	0.76	1	1.25	2.53	2.92	15.7	N/A	-0.01	N/A
0	-0.98	1	1.40	2.02	1.73	14.1	0.01	-0.01	187
0	-1.01	-1	1.42*	1.60	1.67*	4.4*	0.07	0.07*	6.3*
-1	0.19	1	1.42*	2.28	2.13*	6.6*	0.01	0.02*	14.8*
-1	0.22	1	1.43*	2.48	2.13*	14.1*	0.01	0.02*	14.9*
-1	-0.73	1	1.59*	2.28	1.86*	18.5*	0.01	0.01*	24.2*
-1	-0.77	-1	1.61*	1.42	1.90*	34.3*	0.15	0.26*	76.9*
1	0.78	1	1.61*	2.25	3.86*	71.7*	0.007	0.03*	334*
1	-0.86	1	1.65*	2.29	2.05*	10.2*	0.007	0.05*	648*
-1	-0.95	-1	1.70*	1.57	1.94*	23.1*	0.11	0.25*	119*
-1	0.97	1	1.71*	2.59	2.16*	16.5*	0.01	0.01*	35.7*
1	-1.06	1	1.76*	1.72	1.78*	3.4*	0.006	0.05*	752*
1	-1.12	-1	1.80*	1.53	1.48*	3.2*	0.02	-0.02*	181*
-1	-1.17	1	1.83*	1.87	1.64*	12.1*	0.008	-0.001*	114*

* = extrapolated value

A comparison of the residual indentation depth measurements with the regression values indicates that the response surface (equation 18) yields poor estimates of the actual facesheet indentation due to impact, particularly when extrapolating outside of the spherical domain of the test matrix design. As mentioned earlier, this may be understandable given the relative lack of reproducibility in the experimental damage depth measurements for a given test configuration and the disparity between the maximum and minimum facesheet indentation measurements over the range of test configurations. The interpolated response surface (equation 18) estimates, however, do correlate moderately well with the independent experimental measurements for the two cases where the combination of test parameters leads to residual facesheet indentations that are significant in comparison to the sandwich composite stack-up thickness (d = 0.11, 0.13 in; core thickness, X_3 = 3/4 in). Response surfaces similar to equation 18 may be useful in identifying those combinations of material and impact parameters leading to visually detectable damage.

2.2.2 Key Observations.

In the second part of this investigation, the coupled influence of the number of facesheet plies, impact energy, and impactor diameter on the impact damage induced was evaluated using empirically based response surfaces for sandwich composites comprised of carbon-epoxy woven fabric facesheets and Nomex honeycomb cores. The core density, core thickness, and impact velocity were held fixed in this examination. Response surface estimates of the size of the planar damage region (equation 17) suggest that increasing the impactor diameter generally results in a decrease in the damage resistance properties (i.e., the size of the planar region typically associated with core crushing is increased). Given that an increase in the planar damage area is often accompanied by a corresponding decrease in residual strength [5], consideration of various sized impactors is an important part of developing a damage tolerance plan for sandwich composites. An increase in the number of facesheet plies tended to result in an increase in the estimated planar damage dimension for a given set of impact parameters. An increase in the impact energy generally resulted in an increase in the size of the planar damage region for those combinations of facesheet configuration and impactor diameters where facesheet penetration was likely not a concern. Response surface results suggest that the residual facesheet indentation (equation 18) is generally a decreasing function of the number of facesheet plies and impactor diameter for a given impact energy level.

2.3 INFLUENCE OF FACESHEET THICKNESS, IMPACT ENERGY, AND IMPACT VELOCITY ON THE IMPACT DAMAGE RESISTANCE OF SANDWICH COMPOSITES.

In the final study, the isolated effects of the number of facesheet plies (X_1), impact energy (X_4), and impact velocity (X_6) on the damage resistance characteristics of sandwich composite panels are investigated using the Box-Behnken experimental design. Here, different impact velocities leading to a specified value of impact energy were obtained by varying the impactor mass and drop height during impact testing [5]. This effort aims to help clarify the influence of dynamic effects on the damage resistance properties of the given sandwich composites over a range of relatively low-velocity impacts. Table 9 summarizes the low, midrange, and high levels of the natural (X_1, X_4, X_6) and coded (x_1, x_4, x_6) independent variables considered in this effort. Here, the core density ($X_2 = 3.0$ lb/ft^3), core thickness ($X_3 = 3/4$ in), and impactor diameter ($X_5 = 3.0$ in) were held fixed.

TABLE 9. NATURAL VALUES AND CORRESPONDING CODED LEVELS OF THE SANDWICH CONFIGURATION AND IMPACT VARIABLES

i	Independent Variable	Natural Value, X_i	Coded Level, x_i
1	Number of Facesheet Plies	2 [90/45]$_1$	-1
		4 [90/45]$_2$	0
		6 [90/45]$_3$	+1
4	Impact Energy	90.0 in-lb	-1
		120 in-lb	0
		150 in-lb	+1
6	Impact Velocity	65.2 in/sec	-1
		96.3 in/sec	0
		127 in/sec	+1

42

Table 10 summarizes the combinations of coded independent variables as well as the experimentally measured damage sizes for the 15 experiments (tests 31-45) used in the regression analysis. Following the procedure outlined earlier, statistically reliable, second-order response surfaces were generated that characterize the impact damage induced as a function of the number of facesheet plies, impact energy, and impact velocity. An estimate of the diameter of the planar damage region associated with TTU C-scan measurements from the regression analysis may be expressed either in terms of coded or natural values of the independent variables, i.e.,

$$\hat{D} = 2.078 + 0.1483 \cdot x_1 + 0.3768 \cdot x_4 - 0.06175 \cdot x_6$$
$$\dots + 0.01717 \cdot x_1^2 + 0.01617 \cdot x_4^2 + 0.7067 \cdot x_6^2 \qquad \text{(in)} \qquad \text{(19a)}$$
$$\dots - 0.04800 \cdot x_1 \cdot x_4 + 7.500 \cdot 10^{-3} \cdot x_1 \cdot x_6 + 0.02300 \cdot x_4 \cdot x_6$$

and

$$\hat{D} = 7.516 + 0.1242 \cdot X_1 + 9.073 \cdot 10^{-3} \cdot X_4 - 0.1461 \cdot X_6$$
$$\dots + 4.292 \cdot 10^{-3} \cdot X_1^2 + 1.796 \cdot 10^{-5} \cdot X_4^2 + 7.306 \cdot 10^{-4} \cdot X_6^2 \qquad \text{(in)} \qquad \text{(19b)}$$
$$\dots - 8.000 \cdot 10^{-4} \cdot X_1 \cdot X_4 + 1.206 \cdot 10^{-4} \cdot X_1 \cdot X_6 + 2.465 \cdot 10^{-5} \cdot X_4 \cdot X_6$$

TABLE 10. COMPARISONS BETWEEN PREDICTED AND MEASURED DAMAGE SIZES
(From tests 31 to 45)

Test, k	x_1	x_4	x_6	Measured Damage Diameter, D (in)	Predicted Damage Diameter, $\hat{D}$ (in)	$\left\|\dfrac{D-\hat{D}}{D}\right\|$ (%)	Measured Damage Depth, d (in)	Predicted Damage Depth, $\hat{d}$ (in)	$\left\|\dfrac{d-\hat{d}}{d}\right\|$ (%)
31	+1	+1	0	2.25	2.58	14.8	0.007	0.006	8.9
32	+1	-1	0	1.72	1.93	12.0	0.006	0.004	35.4
33	-1	+1	0	2.59	2.38	8.0	0.010	0.012	21.2
34	-1	-1	0	1.87	1.53	17.8	0.008	0.009	7.8
35	+1	0	+1	3.13	2.89	7.6	0.008	0.008	0.0
36	+1	0	-1	3.30	3.0	9.2	0.010	0.013	27.5
37	-1	0	+1	2.28	2.58	13.3	0.017	0.014	16.2
38	-1	0	-1	2.48	2.72	9.6	0.017	0.017	0.0
39	0	+1	+1	3.23	3.13	3.0	0.004	0.005	15.6
40	0	+1	-1	3.24	3.21	1.0	0.018	0.016	11.8
41	0	-1	+1	2.30	2.33	1.3	0.007	0.009	30.4
42	0	-1	-1	2.41	2.50	4.0	0.006	0.005	10.4
43	0	0	0	2.13	2.07	2.5	0.003	0.005	55.6
44	0	0	0	2.04	2.07	1.6	0.007	0.005	33.3
45	0	0	0	2.05	2.07	1.1	0.004	0.005	16.7

The constant term (b_0 = 2.07 in) in equation 19a represents the mean diameter of the TTU C-scan image for those panels corresponding to the center point of the design. Consistent with earlier observations, increasing the number of facesheet plies, x_1, and impact energy, x_4, from their midrange values in equation 19a will result in a linear increase in the predicted response, whereas increasing the impact velocity, x_6, will result in a somewhat smaller linear decrease in the estimated planar damage dimension from b_0. Note that the quadratic term involving the impact velocity contributes significantly to the estimated response (i.e., the midrange velocity defines a relative minimum or "well" in the predicted response). Similar arguments can be made when interpreting the influence of the remaining quadratic and coupling terms in equation 18a on the estimated damage size.

Analogously, an estimate of the maximum residual facesheet indentation from the regression analysis may be expressed either in terms of coded or natural values of the independent variables, i.e.,

$$
\hat{d} = \big[4.667 - 2.625 \cdot x_1 + 1.500 \cdot x_4 - 1.875 \cdot x_6
$$
$$
... + 3.667 \cdot x_1^2 - 0.5833 \cdot x_4^2 + 4.667 \cdot x_6^2 \qquad \text{(in)} \qquad (20a)
$$
$$
... - 0.2500 \cdot x_1 \cdot x_4 - 0.5000 \cdot x_1 \cdot x_6 - 3.750 \cdot x_4 \cdot x_6 \big] \cdot 10^{-3}
$$

and

$$
\hat{d} = 8.257 \cdot 10^{-3} - 7.372 \cdot 10^{-3} \cdot X_1 + 6.093 \cdot 10^{-3} \cdot X_4 - 4.751 \cdot 10^{-4} \cdot X_6
$$
$$
... + 9.167 \cdot 10^{-4} \cdot X_1^2 - 6.481 \cdot 10^{-7} \cdot X_4^2 + 4.825 \cdot 10^{-6} \cdot X_6^2 \qquad \text{(in)} \qquad (20b)
$$
$$
... - 4.167 \cdot 10^{-6} \cdot X_1 \cdot X_4 - 8.039 \cdot 10^{-6} \cdot X_1 \cdot X_6 - 4.019 \cdot 10^{-6} \cdot X_4 \cdot X_6
$$

The constant term (b_0 = 0.004 in) in equation 20a represents the mean value of the peak residual facesheet indentation for the three center runs. The magnitudes of the coefficients of the linear terms in equation 19a suggest an increase in the number of facesheet plies, x_1, or impact velocity, x_6, will result in a linear decrease in the predicted response at points removed from the center point of the test matrix, while an increase in the impact energy, x_4, will tend to produce a linear increase in the estimated response. Analogous arguments can be made when interpreting the influence of the remaining terms in equation 19a on the predicted response.

2.3.1 Discussion of Facesheet Configuration and Impact Parameter Regression Model Results.

Table 10 also summarizes the measured and predicted planar damage diameter and the maximum residual facesheet indentation for each of the sandwich composite panels considered in this effort. The difference between the experimentally measured damage diameters and the estimated values using equation 19 varied between 1.0% and 17.8% for the 15 panels tested (tests 31-45), with a mean difference of 7.1%. This suggests that the response surface (equation 19) provides a reasonable characterization of the influence of the number facesheet plies, impact energy, and impact velocity on the planar size of the internal damage generated due to impact. The regression results may also be viewed schematically in the space of coded independent variables as shown in figure 25.

3.247
3.216

2.594
2.387

2.254
2.588

3.235
3.139

2.078

3.307
3.004

x_4 = Coded impact
energy

2.485
2.722

3.133
2.895

2.281
2.584

2.412
2.509

x_1 = Coded number of
facesheet plies

x_6 = Coded impact
velocity

1.872
1.538

1.724
1.930

2.308
2.339

D = Measured damage diameter (*in*)
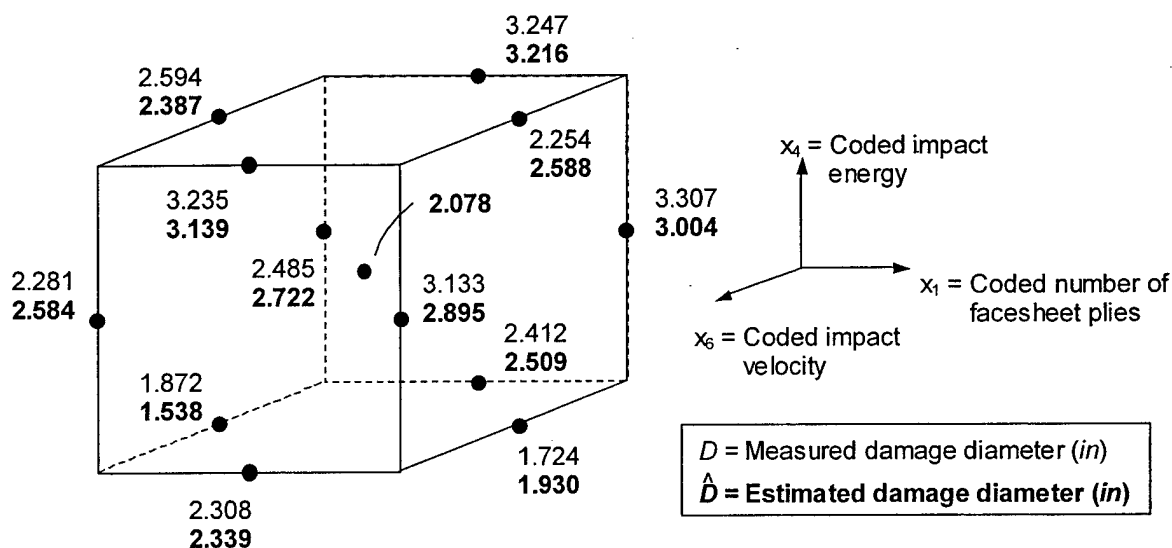
$\hat{D}$ = **Estimated damage diameter (*in*)**

FIGURE 25. RESPONSE SURFACE ESTIMATES OF THE INTERNAL DAMAGE DIAMETER AS A FUNCTION OF SANDWICH CONFIGURATION AND IMPACT PARAMETERS

From table 10, a number of the actual peak residual facesheet indentations approached the limits of mechanical measurement and generally were on the order of the ply thickness (i.e., $d = 0.003$-0.01 in); lack of reproducibility in the experimental measurements at the center point of the design was also a concern. Similar to the first study discussed in section 2.1, the magnitudes of the differences between the measured and estimated indentation depths were reasonably small in comparison to the typical ply thickness. The percentage difference between the two values, however, was fairly significant, especially for particularly shallow indentations. Hence, the response surface estimate (equation 20) is likely inaccurate for the class of blunt-object impacts considered here as response surface was constructed with fixed impact diameter of 3.0 in.

Figures 26 through 31 summarize the influence of the number of facesheet plies (X_1, x_1), impact energy (X_4, x_4), and impact velocity (X_6, x_6) on the estimated size of the planar damage region. Figures 26, 28, and 30 each contain three response surface contour plots for the cases where the impact velocity, impact energy, and number of facesheet plies, respectively, are varied between low, midrange, and high values. It is clear from figures 26(a) through 26(c), that the estimated planar damage diameter is generally an increasing function of the number of facesheet plies and impact energy. A comparison of the three plots reveals that the minimum damage size for a given combination of facesheet configuration and impact energy occurs at the midrange impact velocity, $X_6 = 96.3$ in/sec (or $x_6 = 0$). This effect is more apparent in figures 28 and 30 where the contour plots are very nearly symmetric about minimum values occurring in the vicinity of the line, $X_6 = 96.3$ in/sec. The magnitude of the estimated damage size can increase appreciably as the impact velocity is varied from the midrange test value ($x_6 = 0$) to either high or low values ($x_6 = \pm 1$). The response surface estimates are in general agreement with the experimental observations.
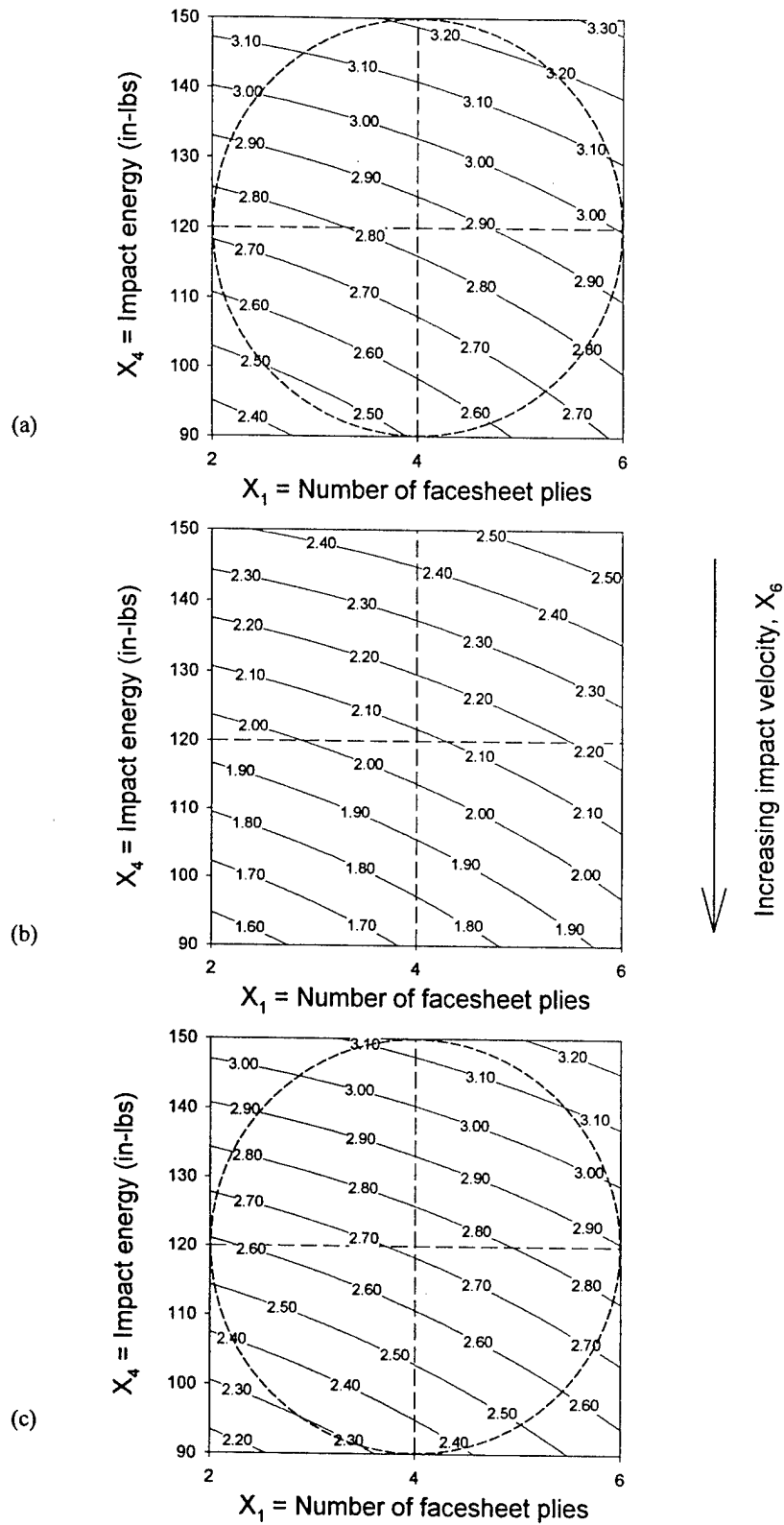
45

FIGURE 26. PREDICTED DAMAGE DIAMETER (in): (a) X_6 = 65.2 in/sec; (b) X_6 = 96.3 in/sec; and (c) X_6 = 127 in/sec

$$\begin{Bmatrix} x_1 \\ x_4 \\ x_6 \end{Bmatrix} = \begin{Bmatrix} -1 \\ +1 \\ 0 \end{Bmatrix}$$

TEST # 33 $D = 2.594\ in$

Increasing facesheet thickness, x_1

$$\begin{Bmatrix} x_1 \\ x_4 \\ x_6 \end{Bmatrix} = \begin{Bmatrix} +1 \\ +1 \\ 0 \end{Bmatrix}$$

TEST # 31 $D = 2.254\ in$

Increasing facesheet thickness and impact energy.

Increasing impact energy, x_4

$$\begin{Bmatrix} x_1 \\ x_4 \\ x_6 \end{Bmatrix} = \begin{Bmatrix} 0 \\ 0 \\ 0 \end{Bmatrix}$$

TEST # 43 $D = 2.131\ in$

$$\begin{Bmatrix} x_1 \\ x_4 \\ x_6 \end{Bmatrix} = \begin{Bmatrix} 0 \\ 0 \\ 0 \end{Bmatrix}$$

TEST # 45 $D = 2.056\ in$

Increasing impact energy, x_4

$$\begin{Bmatrix} x_1 \\ x_4 \\ x_6 \end{Bmatrix} = \begin{Bmatrix} 0 \\ 0 \\ 0 \end{Bmatrix}$$

TEST # 44 $D = 2.046\ in$

$b_0 = 2.078\ in$

Increasing facesheet thickness and impact energy.

$$\begin{Bmatrix} x_1 \\ x_4 \\ x_6 \end{Bmatrix} = \begin{Bmatrix} -1 \\ -1 \\ 0 \end{Bmatrix}$$

TEST # 34 $D = 1.872\ in$

Increasing facesheet thickness, x_1

$$\begin{Bmatrix} x_1 \\ x_4 \\ x_6 \end{Bmatrix} = \begin{Bmatrix} +1 \\ -1 \\ 0 \end{Bmatrix}$$

TEST # 32 $D = 1.724\ in$
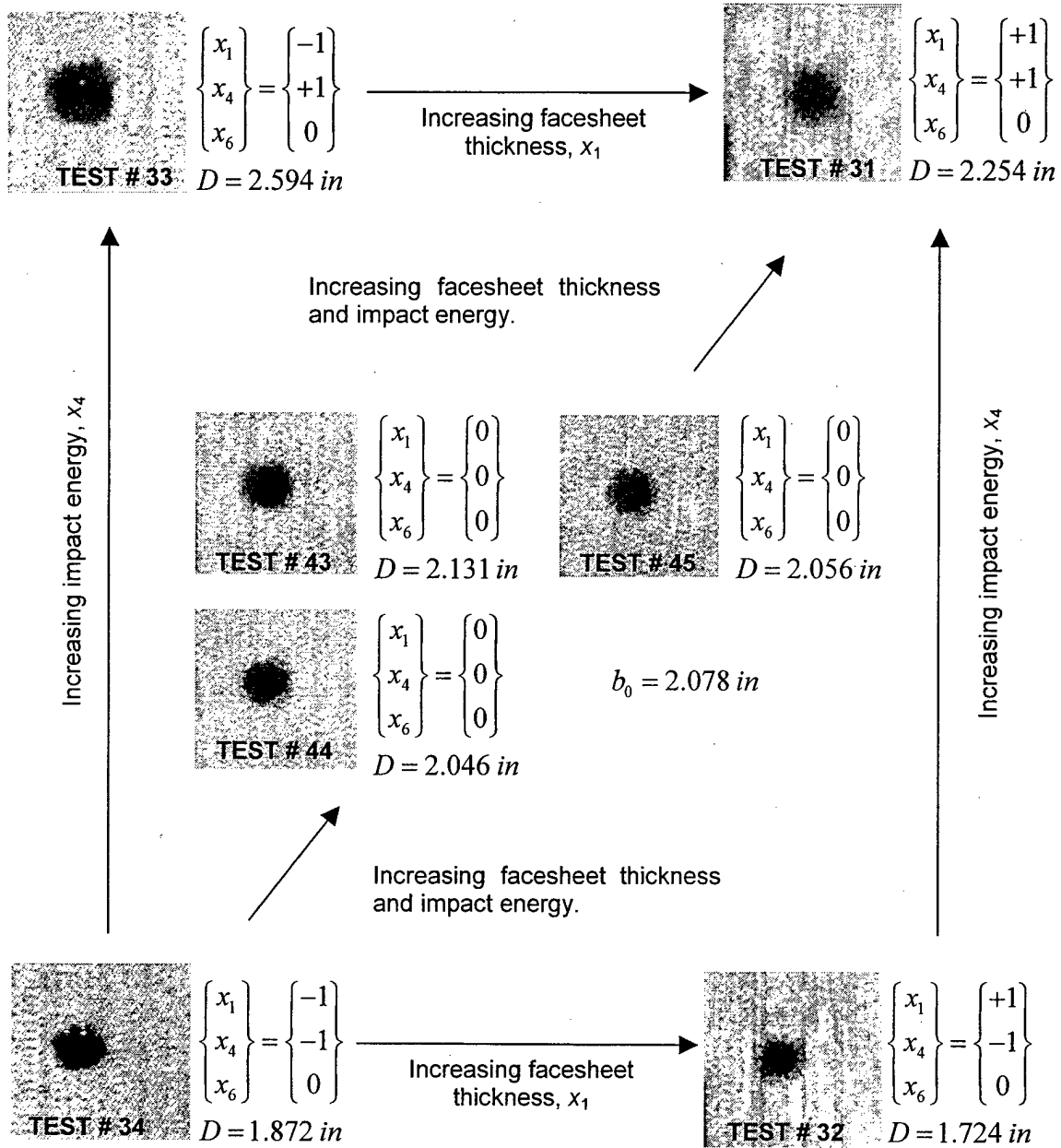
FIGURE 27. MEASURED DAMAGE DIAMETER FOR IMPACT VELOCITY,
$X_6 = 96.3$ in/sec ($x_6 = 0$)

Figures 27, 29, and 31 show the TTU C-scan images and recorded damage diameters for the test configurations involving the midrange impact velocity ($x_6 = 0$; $X_6 = 96.3$ in/sec), impact energy level ($x_4 = 0$; $X_4 = 120$ in-lb), and facesheet configuration ($x_1 = 0$; $X_1 = 4$ plies) that are consistent with the regressions shown in figures 26(b), 28(b), and 30(b), respectively. Sandwich panel stiffness properties, energy absorption capability, and support boundary conditions all likely play a key role in the dynamic impact response leading to damage development. This underscores the importance of adequately characterizing the expected impact scenarios when establishing a damage tolerance plan for sandwich composite aircraft structures.
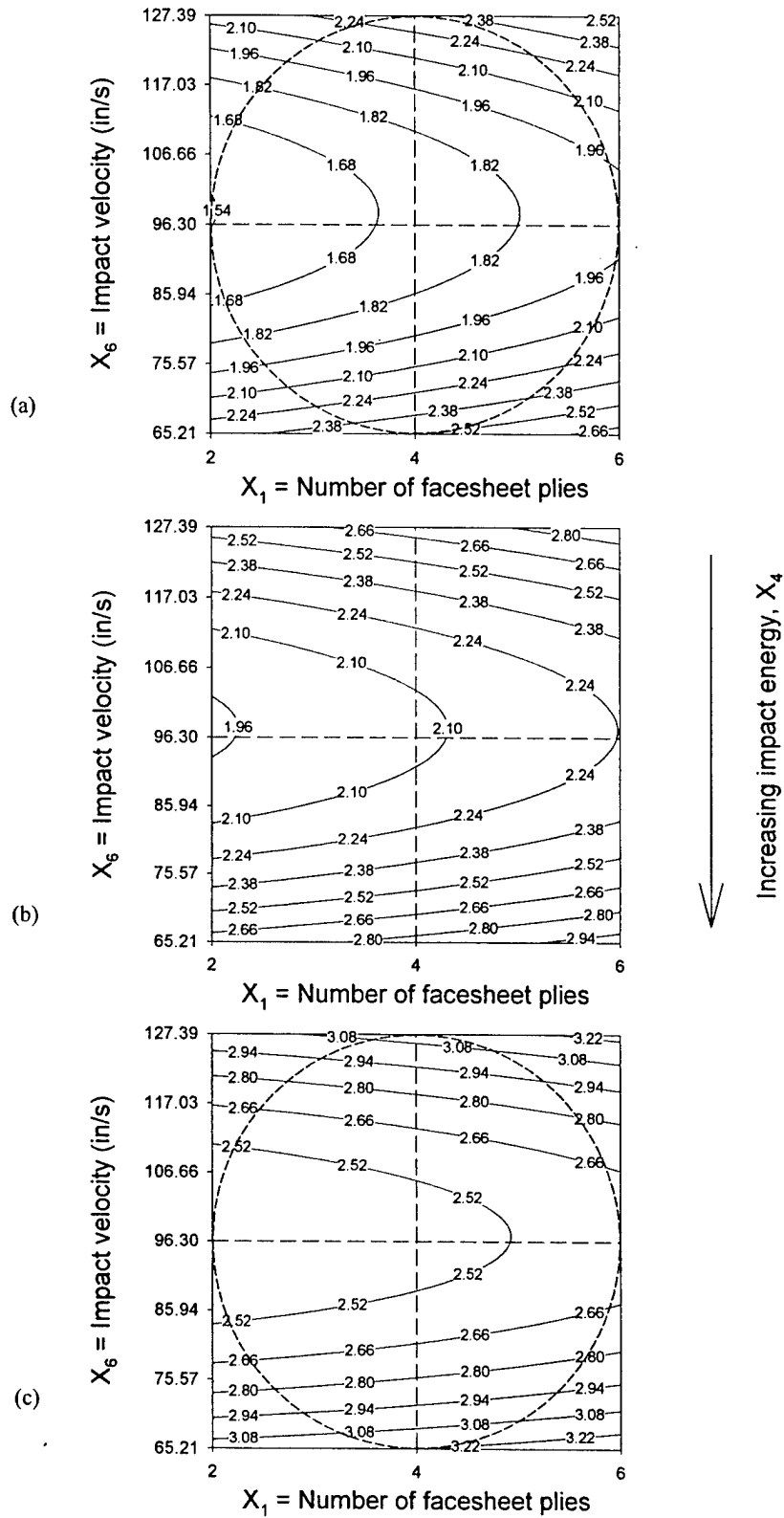
47

FIGURE 28. PREDICTED DAMAGE DIAMETER (in): (a) X_4 = 90.0 in-lb;
(b) X_4 = 120 in-lb; and (c) X_4 = 150 in-lb

$\begin{Bmatrix} x_1 \\ x_4 \\ x_6 \end{Bmatrix} = \begin{Bmatrix} -1 \\ 0 \\ +1 \end{Bmatrix}$

TEST # 37 $D = 2.281\ in$

Increasing facesheet thickness, x_1

TEST # 35 $D = 3.133\ in$

$\begin{Bmatrix} x_1 \\ x_4 \\ x_6 \end{Bmatrix} = \begin{Bmatrix} +1 \\ 0 \\ +1 \end{Bmatrix}$

Increasing facesheet thickness and impact velocity.

Increasing impact velocity, x_6

TEST # 43 $D = 2.131\ in$

$\begin{Bmatrix} x_1 \\ x_4 \\ x_6 \end{Bmatrix} = \begin{Bmatrix} 0 \\ 0 \\ 0 \end{Bmatrix}$

TEST # 45 $D = 2.056\ in$

$\begin{Bmatrix} x_1 \\ x_4 \\ x_6 \end{Bmatrix} = \begin{Bmatrix} 0 \\ 0 \\ 0 \end{Bmatrix}$

Increasing impact velocity, x_6

TEST # 44 $D = 2.046\ in$

$\begin{Bmatrix} x_1 \\ x_4 \\ x_6 \end{Bmatrix} = \begin{Bmatrix} 0 \\ 0 \\ 0 \end{Bmatrix}$

$b_0 = 2.078\ in$

Increasing facesheet thickness and impact velocity.

TEST # 38 $D = 2.485\ in$

$\begin{Bmatrix} x_1 \\ x_4 \\ x_6 \end{Bmatrix} = \begin{Bmatrix} -1 \\ 0 \\ -1 \end{Bmatrix}$

Increasing facesheet thickness, x_1

TEST # 36 $D = 3.307\ in$

$\begin{Bmatrix} x_1 \\ x_4 \\ x_6 \end{Bmatrix} = \begin{Bmatrix} +1 \\ 0 \\ -1 \end{Bmatrix}$

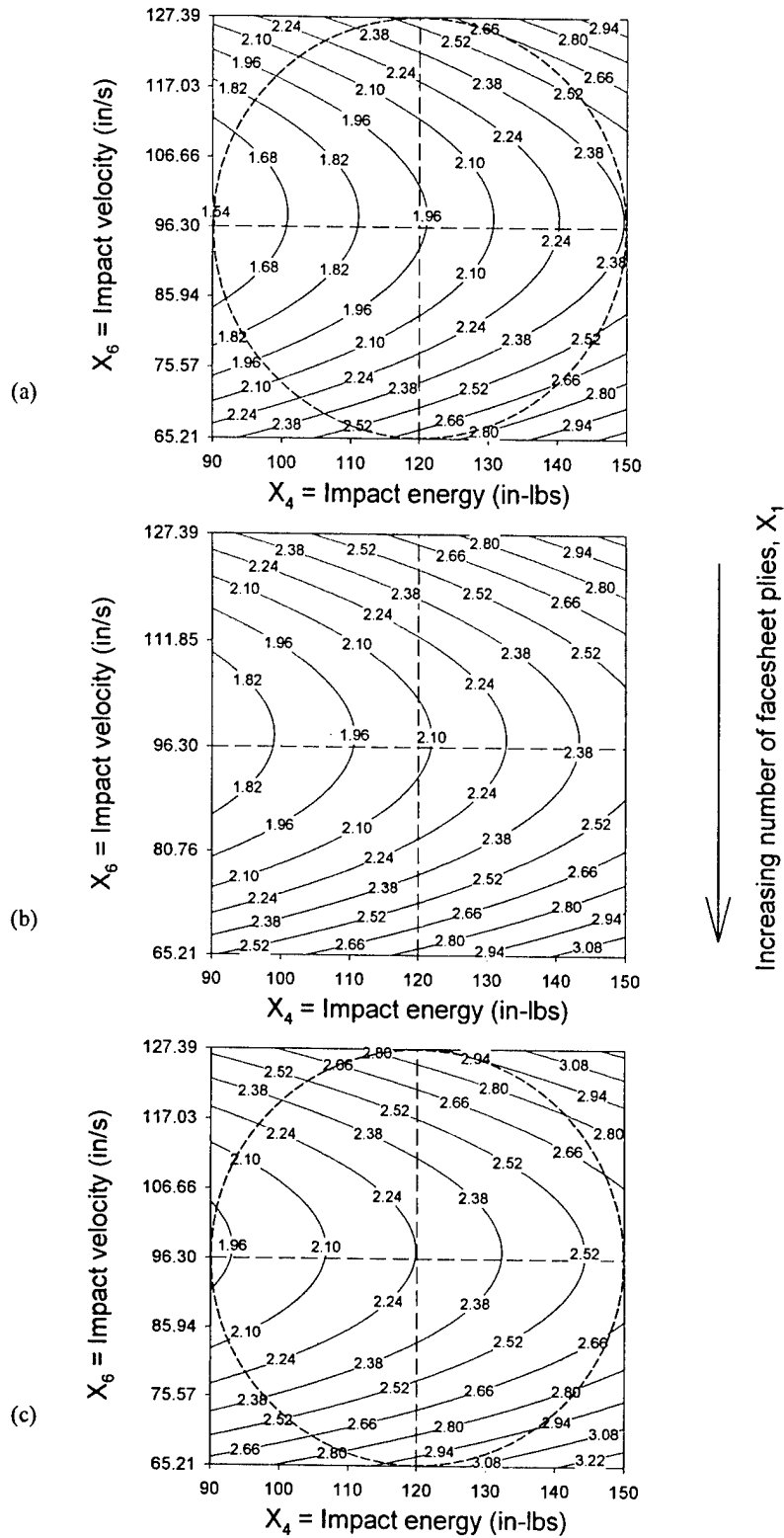FIGURE 29. MEASURED DAMAGE DIAMETER FOR IMPACT ENERGY, $X_4 = 120$ in-lb ($x_4 = 0$)

FIGURE 30. PREDICTED DAMAGE DIAMETER (in): (a) X_1 = 2 plies $[90/45]_1$; (b) X_1 = 4 plies $[90/45]_2$; and (c) X_1 = 6 plies $[90/45]_3$
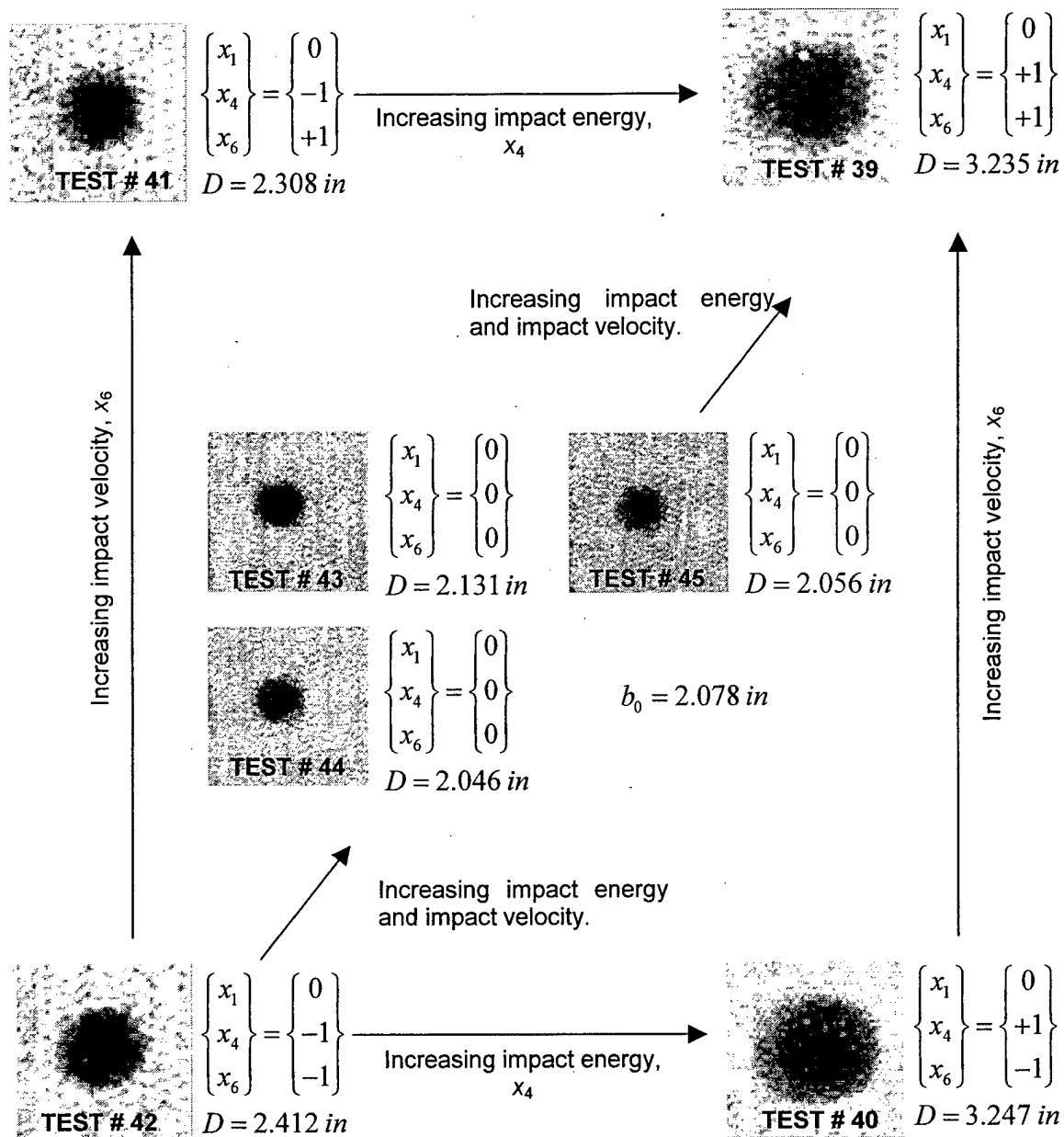
FIGURE 31. MEASURED DAMAGE DIAMETER FOR FACESHEET CONFIGURATION,
$X_1 = 4$ plies $[90/45]_2$ $(x_1 = 0)$

Figures 32 through 34 summarize the influence of the number of facesheet plies, impact energy, and impact velocity on the estimated maximum residual facesheet indentation. While using the response surface (equation 20) is inappropriate to estimate particularly shallow residual facesheet indentations, it may be helpful in identifying those combinations of material and impact parameters that lead to the maximum surface damage. Figures 32, 33, and 34 each contain three response surface contour plots for the cases where the impact velocity, impact energy, and number of facesheet plies, respectively, are varied between low, midrange, and high values. Not surprisingly, the maximum estimated residual facesheet indentation for a given combination of impact energy and impact velocity generally occurred for the 2-ply facesheet configuration. While the estimated damage depth tended to be an increasing function of impact energy, the regression results were somewhat sensitive to the impact velocity. For higher energy impacts ($X_4 \approx 150$ in-lb), the maximum damage occurred where the impact velocity was a relative minimum (see figure 34). For decreasing impact energy levels, however, the minimum facesheet damage generally occurred in the vicinity of the midrange velocity ($X_6 \approx 96.3$ in/sec). The impact parameter coupling is evident from the formation of a relative minimum in the contour plots shown in figure 34, as well as in the magnitude of the coefficient in the coupling term ($x_4 \cdot x_6$) in equation 20. Such influences would be relatively difficult to discern using standard single-variable testing strategies. These trends are generally consistent with the experimental observations (see table 10). As a central aspect of this work, a critical comparison of figures 26, 28, and 30 to figures 32, 33, and 34 suggests that those combinations of material and impact parameters that lead to the maximum amount of internal damage do not correspond to the configurations that produce the greatest facesheet indentation. Again, this may allow for the design tailoring of sandwich composites to enhance the damage resistance/tolerance characteristics for a range of expected impact events.

Table 11 contains a limited set of additional independent experimental results from Tomblin, et al. [5], where the combination of configuration and impact variables lie within the spherical domain of the test matrix design used in this study. Response surface estimates of the planar diameter of the internal damage (equation 19) and the residual facesheet indentation (equation 20) are summarized in table 11. The difference between the experimentally measured damage diameters and the interpolated values varied between 1.5% and 27.2%, with a mean difference of 13.0%. Hence, the response surface (equation 19) correlates moderately well with the experimental data within the space of the Box-Behnken design. Again, this suggests that response surfaces similar to equation 19 may be useful tools in identifying combinations of sandwich composite material/design parameters leading to improved damage resistance properties for a given class of impact. A comparison of the residual indentation depth measurements with the regression values indicates that the response surface (equation 20) yields somewhat poor estimates of the actual facesheet indentation due to impact.
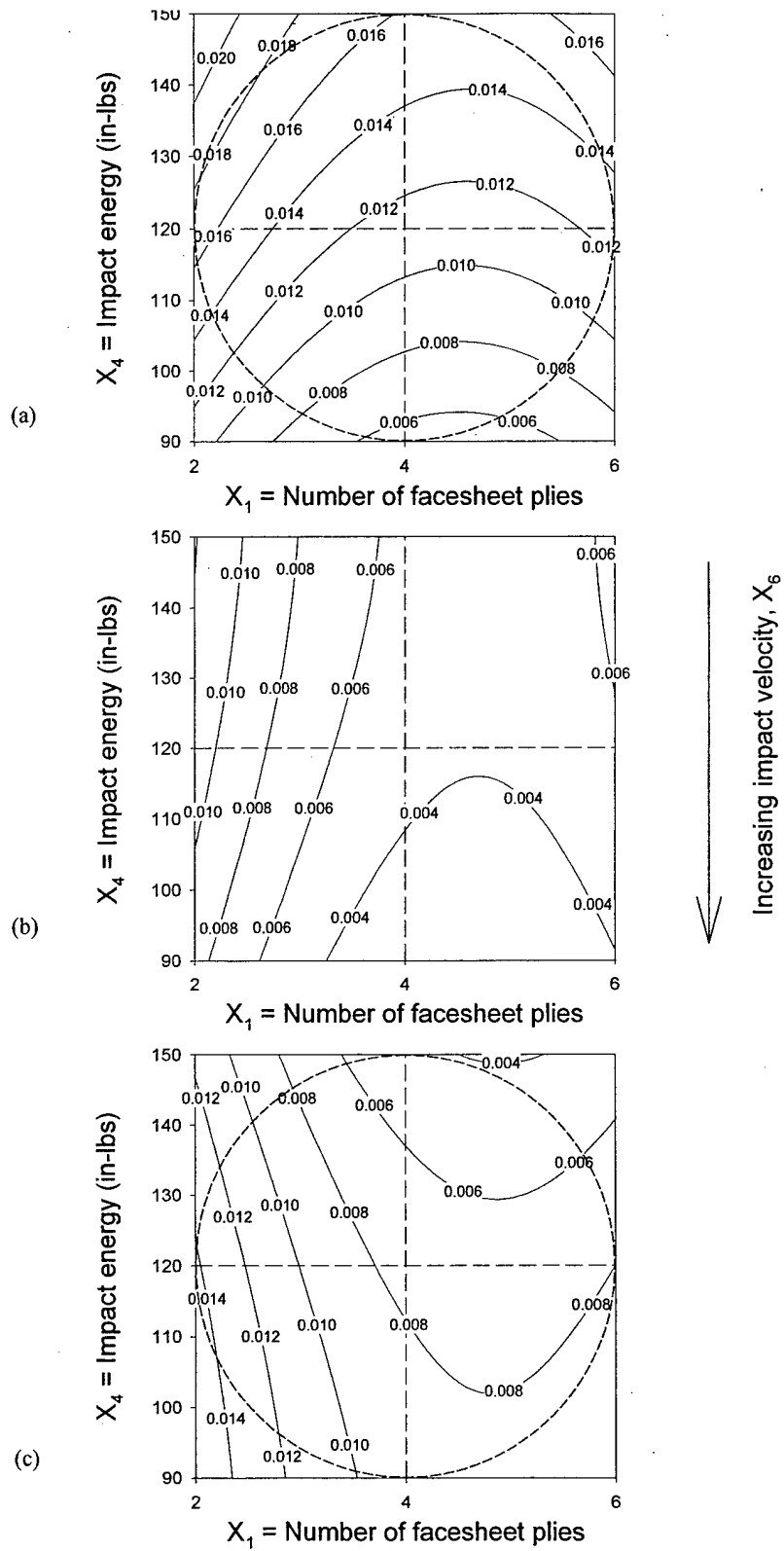
FIGURE 32. PREDICTED RESIDUAL INDENTATION DEPTH (in): (a) X_6 = 65.2 in/sec; (b) X_6 = 96.3 in/sec; and (c) X_6 = 127 in/sec
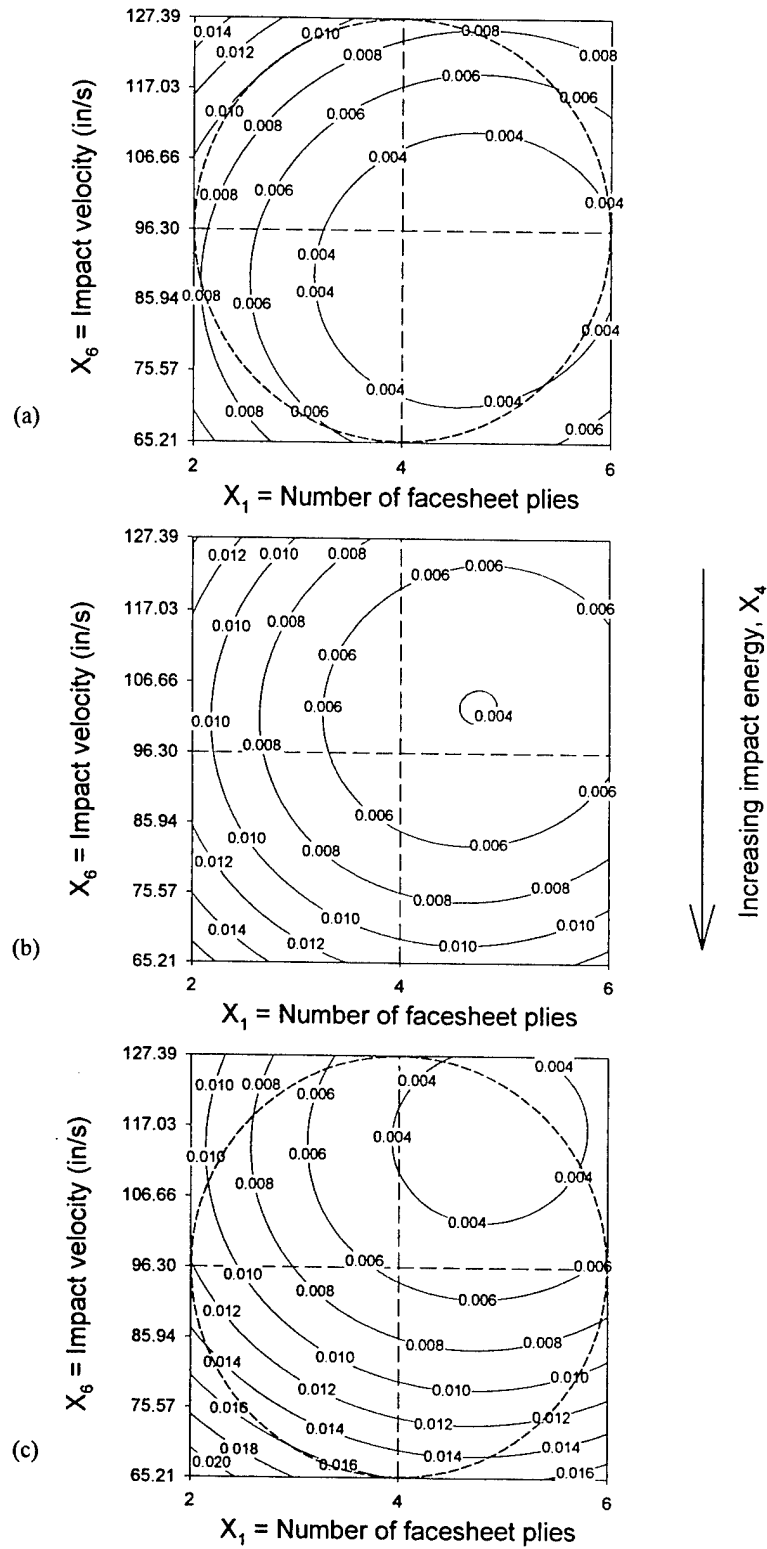
FIGURE 33. PREDICTED RESIDUAL INDENTATION DEPTH (in): (a) X_4 =90.0 in-lb; (b) X_4 = 120 in-lb; and (c) X_4 = 150 in-lb
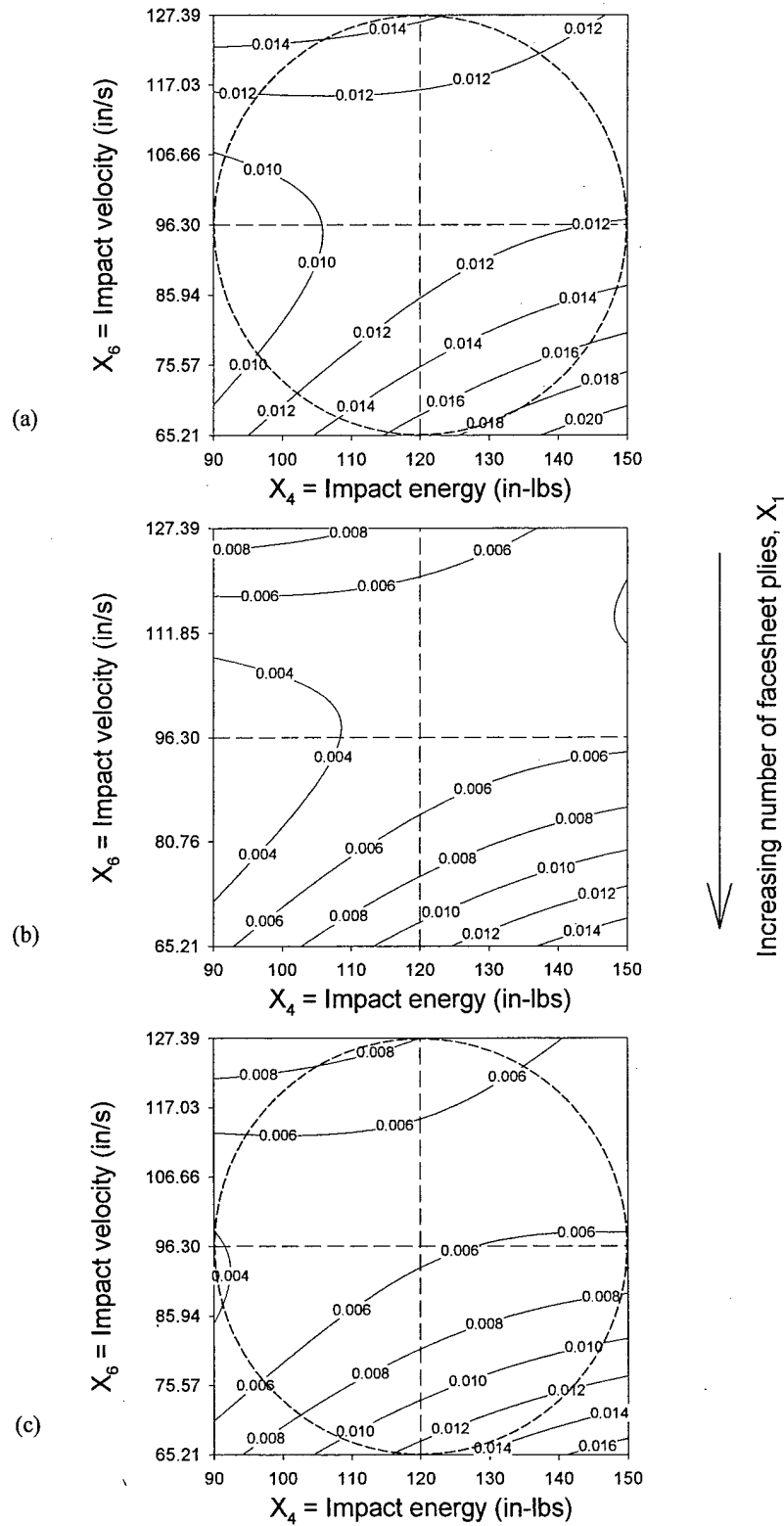
54

FIGURE 34. PREDICTED RESIDUAL INDENTATION DEPTH (in): (a) $X_1 = 2$ plies [90/45]$_1$; (b) $X_1 = 4$ plies [90/45]$_2$; and (c) $X_1 = 6$ plies [90/45]$_3$

TABLE 11. INTERPOLATION OF REGRESSION RESULTS IN THE SPACE OF CODED SANDWICH CONFIGURATION AND IMPACT VARIABLES

x_1	x_4	x_5	r	Measured Damage Diameter, D (in)	Predicted Damage Diameter, $\hat{D}$ (in)	$\left\|\dfrac{D-\hat{D}}{D}\right\|$ (%)	Measured Damage Depth, d (in)	Predicted Damage Depth, $\hat{d}$ (in)	$\left\|\dfrac{d-\hat{d}}{d}\right\|$ (%)
0	0.30	-0.23	0.37	2.85	2.24	21.4	0.026	0.006	76.6
0	0.76	-0.08	0.76	2.53	2.38	5.9	N/A	0.006	N/A
0	-0.98	-0.14	0.99	2.02	1.75	13.5	0.013	0.002	80.9
-1	0.04	-0.02	1.0	1.99	1.96	1.5	0.014	0.011	21.1
-1	0.50	-0.11	1.12	2.78	2.17	21.8	0.027	0.012	55.2
1	0.63	-0.07	1.18	2.58	2.46	4.8	0.008	0.007	17.4
0	-1.18	-0.13	1.18	1.80	1.67	7.1	0.005	0.002	63.4
-1	-0.73	-0.11	1.24	2.28	1.66	27.2	0.013	0.009	28.6
1	-0.86	-0.07	1.32	2.29	1.98	13.5	0.007	0.004	40.5

2.3.2 Key Observations.

In the final part of this investigation, the coupled influence of the number of facesheet plies, impact energy, and impact velocity on the impact damage induced was evaluated using empirically based response surfaces for sandwich composites comprised of carbon-epoxy woven fabric facesheets and Nomex honeycomb cores; the core density, core thickness, and impactor diameter were held fixed in this examination. Response surface estimates of the size of the planar damage region typically associated with core crushing (equation 19) suggest that the damage development is somewhat sensitive to the velocity of the impactor; midrange values of impact velocity resulted in damage estimates that were a relative minimum. Similar to earlier results, an increase in the number of facesheet plies and/or impact energy tended to result in an increase in the estimated planar damage dimension for a given set of impact parameters. Response surface results suggest that the residual facesheet indentation (equation 20) due to impact is also impact velocity dependent. However, as the response surface was constructed on the basis of 3.0-in diameter impactor (shallow indents) the validity of equation 20 is questionable.

3. CONCLUSIONS AND RECOMMENDATIONS.

In this investigation, the influence of sandwich configuration and impact parameters on the damage resistance characteristics of sandwich composites comprised of carbon-epoxy woven fabric facesheets and Nomex honeycomb cores were evaluated using empirically based response surfaces. A series of carefully selected tests were used to isolate the coupled influence of the number of facesheet plies, core density, core thickness, impact energy, impactor diameter, and impact velocity on the damage induced in sandwich composites due to impact normal to the surface and with relatively blunt spherical steel indentors. The ranges of selected sandwich configuration were typical of those found in aircraft applications. The diameter of the planar damage area, determined using through transmission ultrasonic (TTU) C-scan measurements of

impacted sandwich panels and the maximum residual facesheet indentation depth, were used to describe the extent of impact damage. Earlier studies have suggested that TTU C-scan measurements can be used to characterize the region over which Nomex honeycomb cell wall buckling and fracture occurs; such damage can occur in the absence of significant surface damage and may lead to drastic reductions in compression after impact (CAI) residual strength. Estimates of the size of the planar damage region and residual facesheet indentation, as a function of material system and impact parameters that were made using quadratic response surfaces, correlated reasonably well with experimentally determined values.

For a fixed set of impact parameters, estimates, made using response surface, of the size of the internal planar damage region and residual facesheet indentation show that impact damage development is highly sandwich-configuration dependent. Estimates of the size of the planar damage region suggest that increasing the thickness of the core results in the greatest improvement in the damage resistance properties (i.e., the size of the planar region typically associated with core crushing is reduced). Independently increasing the number of facesheet plies and/or core density generally resulted in an increase in the size of the estimated internal damage, although simultaneously varying these parameters could result in either an improvement or degradation in the impact damage resistance properties. Changes in sandwich configurations can result in either enhanced or degraded penetration resistance and bending stiffness properties that govern the damage formation. Estimates, made using response surface, for the maximum residual facesheet indentation show that increasing the number of facesheet plies results in the greatest decrease in the predicted surface damage. While such estimates did not necessarily correlate well with experimental data for test configurations with relatively shallow indentations, these estimates may prove useful in determining combinations of material and impact parameters that produce the greatest degree of visible facesheet damage.

In addition, the experimental results and regression analysis suggest that impact damage development in sandwich composites is highly sensitive to the diameter of the impactor, impact energy, and impact velocity. Based upon the response surface estimates, an increase in the diameter of the impactor will result in a significant increase in the planar dimension of the internal damage and a decrease in the residual facesheet indentation, particularly for those sandwich panels with thicker facesheets. This suggests that blunt-object impacts may result in appreciable damage that is not amenable to visual inspection. An increase in the impact energy generally resulted in an increase in the predicted planar damage dimension, with the exception of those combinations of impactor diameter and facesheet configuration where facesheet penetration was a concern. Moreover, response surface results indicate that the damage formation is somewhat sensitive to the velocity of the impactor. Sandwich panel stiffness properties, energy absorption capability, and support boundary conditions all play a key role in the dynamic impact response leading to damage development. Clearly, an accurate characterization of expected impact scenarios should be an important part of the development of a damage tolerance plan for sandwich composites.

The response surface results indicate that those combinations of sandwich configurations and impact parameters leading to the maximum internal damage do not correspond to those that result in the greatest facesheet indentation; such a correlation would be difficult to ascertain using traditional single-variable test strategies and analysis. Using the response surface

methodology outlined here, it may be possible to tailor sandwich composite designs that maximize the degree of detectable facesheet damage while minimizing the internal damage associated with expected impacts. Hence, the response surface technique may potentially be used in the design of sandwich composites with desired damage resistance characteristics.

To fully develop the concepts summarized here, it is important to investigate the damage tolerance aspects of the problem. Future efforts will be aimed at correlating the loss of CAI residual strength with the damage resistance results obtained herein. Of course, it is desirable to investigate other measures of damage formation in addition to those considered in this report. The structural requirements and design criteria must also be reviewed as related to the implications of impact damage resistance studies on surface visibility and internal damage. For example, ultimate load requirements for the threshold of visual detection may force a robust design for some sandwich configurations where residual strength approaches a lower limit before becoming visible. On the other hand, some weight penalty will come from not understanding the proper balance of impact damage resistance and tolerance.

<u>4. REFERENCES.</u>

1. Allen, H.G., *Analysis and Design of Structured Sandwich Panels*, Pergammon Press, Oxford, 1969.

2. Plantema, F.J., *Sandwich Construction*, Wiley & Sons, Chinchester, 1966.

3. Vinson, J.R., *The Behavior of Sandwich Structures of Isotropic and Composite Materials*, Technomic Publications, Lancaster, 1999.

4. Tomblin, J., Lacy T., Smith, B., Hooper, S., Vizzini, A., and Lee, S., "Review of Damage Tolerance for Composite Airframe Structures," Federal Aviation Administration Report Number DOT/FAA/AR-99/49, pp. 1-61, 1999.

5. Tomblin, J.S., Raju, K.S., Liew, J., and Smith, B.L., "Impact Damage Characterization and Damage Tolerance of Composite Sandwich Airframe Structures: Phase I Report," Federal Aviation Administration Report Number DOT/FAA/AR-00/44, 2001.

6. Abrate, S., "Impact on Laminated Composite Materials," *Applied Mechanics Review*, 44(4), pp. 155-190, 1991.

7. Abrate, S., "Impact on Laminated Composites: Recent Advances," *Applied Mechanics Review*, 47(11), pp. 517-544, 1994.

8. Abrate, S., "Localized Impact on Sandwich Structures With Laminated Facings," *Applied Mechanics Review*, 50(2), pp. 69-82, 1997.

9. Russell, S.G., Lin, W., Kan, H.-P., and Deo, R.B., "Damage Tolerance and Fail Safety of Composite Sandwich Panels," *SAE Transactions, Journal of Aerospace*, 103, pp. 2175-2182, 1994.

10. Noor, A.K., Burton, W.S., and Bert, C.W., "Computational Models for Sandwich Panels and Shells," *Applied Mechanics Review*, 49(3), pp. 155-199, 1996.

11. Sierakowski, R.L. and Newaz, G.M., "Damage Tolerance in Advanced Composites," Technomic, Lancaster, 1995.

12. Box, G.E.P. and Behnken, D.W., "Some New Three Level Designs for the Study of Quantitative Variables," *Technometrics*, 2(4), pp. 455-475, 1960.

13. Box, G.E.P., Hunter W.G., and Hunter, J.S., *Statistics For Experiments*, Wiley & Sons, New York, 1978.

14. Montgomery, D.C., *Design and Analysis of Experiments*, Wiley & Sons, New York, 1991.

15. Myers, R. and Montgomery, D.C., *Response Surface Methodology*, Wiley & Sons, New York, 1995.

16. Neter, J., Wasserman W., and Kunter, H.M., "Applied Linear Statistical Models, 3rd edition," *Irwin*, Homewood, IL, 1990.

17. Khuri, A.K. and Cornel, J.A., *Response Surfaces*, Marcel Dekker, Inc., 1987.

18. Saczalski, T.K., "Determination of Multivariable G_{Ic} and G_{IIc} Fracture Toughness Response Functions for Fiber/Resin Composite," Proceedings of the 34th International SAMPE Symposium and Exhibition, pp. 726-736, 1989.

19. Saczalski, T., Lucht, B., and Steeb, D., "Advanced Experimental Design Applied to Damage Tolerance of Composite Materials," Proceedings of the 23rd International SAMPE Conference, Kiamesha Lake, NY, Oct. 21-24, 1991.

20. Saczalski, T., Lucht, B., and Saczalski, K., "Experimental Design Methods for Assessment of Composite Damage in Recreational Structures," *Composite Materials: Fatigue and Fracture*, Vol. 6, pp. 45-69, 1997.